J. Fluid Mech. (1990), *vol.* 214, *pp.* 251–286
Printed in Great Britain

Lubricated pipelining. Part 3 Stability of core–annular flow in vertical pipes

By KANGPING CHEN, RUNYUAN BAI AND DANIEL D. JOSEPH

Department of Aerospace Engineering and Mechanics, University of Minnesota, Minneapolis, MN 55455, USA

(Received 16 March 1989 and in revised form 14 October 1989)

The stability of core–annular flow in vertical pipes is analysed using the linearized theory of stability. In previous studies instabilities due to interfacial friction, interfacial tension and Reynolds stresses in the bulk fluid were identified and associated with observed instabilities. In this study we include and analyse the effects of gravity. In one case gravity opposes and in the other aids the applied pressure gradient. Some preliminary results from our experiments are also presented. The prediction of stability for perfect core–annular flow in a carefully selected window of parameters is verified for the case of free fall in which the applied pressure gradient vanishes.

1. Introduction

This paper is the fourth of a series on the stability of core–annular flow (CAF). In the previous three works, Joseph, Renardy & Renardy (1984, hereinafter referred to as JRR), Preziosi, Chen & Joseph (1989, hereinafter referred to as PCJ) and Hu & Joseph (1989, hereinafter referred to as HJ), gravity was neglected. PCJ calculated growth rates, neutral curves and HJ also calculated the terms in the energy balance. By correlating the profile of instability as calculated by linear theory with experiments, the linear theory can be used as a diagnostic tool predicting flow regimes which arise in practice: bubbles and slugs of oil and water, bubbly mixtures of oil and water, stable CAF, wavy core flow and emulsions of water in oil. Flow regimes, wavelengths and wave speeds seem to be predicted with fair accuracy by linear theory, even with gravity neglected. The apparent success of the linear theory in predicting mechanics deeply in nonlinear regimes is a surprise. In this paper we are going to again carry out a linearized analysis, for Poiseuille flow in vertical pipes in which we can account fully for the effects of gravity in the presence of a density difference without violating the assumption that the basic flow is axisymmetric. We also include the effect of an applied pressure gradient which can reinforce or oppose the body force due to gravity.

Previous works on the stability of core–annular flow are discussed in the three references mentioned. All these works neglect gravity. Gravity does not have an effect on the dynamics when there is just one fluid. Hickox (1971) was the first to treat the effects of gravity in Poiseuille flow of two fluids in a vertical pipe. He also considered the effects of an applied pressure gradient. However, his analysis is limited to the long waves and the case where the more viscous component is in the annulus, which is of little interest to the application of lubricated pipelining. Lister (1987) studied the instability of vertical channel flow of two fluids to long waves in

the limit of very large annulus. Y. Renardy (1987) investigated numerically the stability of lubricated Poiscuille flow of two liquids in a vertical channel to long waves. She noticed that there could be an instability due to the density difference in the presence of gravity even when the viscosities are matched. In this paper we study the stability of vertical core–annular flow in a circular pipe when all the major physical effects, except nonlinear effects and preferential wetting, are included. The major physical effects treated are associated with gravity, density difference, viscosity difference, surface tension and Reynolds number. Our calculations show that heavy lubricant should be used to stabilize capillary instability in slow flows in the direction of gravity and light lubricant should be used for slow flow against gravity. Our results also show that there is an optimal value of density ratio that maximizes the interval of Reynolds numbers for which CAF is stable.

It is essential that the predictions of linearized theory be tested against experiments. We have constructed two devices to study the flow of two liquids in a vertical pipe, one for free-fall flow under gravity and the other for forced flows. We used the linear theory to predict the parameters necessary to enter into the window of stability of perfect core–annular flow in the free fall apparatus and obtained agreement of theory and experiment. With these two devices we hope to monitor all the parameters which appear in the analysis given here and those which are needed for the nonlinear theory we are working out. The vertical pipe seems to be the instrument of choice in this field because the experiments and the analysis are well matched. The analysis of and experiments on bicomponent liquid flow in vertical pipes may help to understand what happens in the pumping of crude oil from underground through a drilled well in the presence of water. In fact water lubrication for well pumping appears to be a possible technology in down hole situations with shallow wells or when the oil viscosity is very large as in cold wells. For such applications pumping up against gravity is the interesting case.

2. Basic flow

Two immiscible liquids are flowing up or down a vertical pipe of radius R_2. The interface between the two liquids is given by $r = R(\theta, x, t)$, where (r, θ, x) are cylindrical coordinates chosen in such a way that gravity is acting in the positive x-direction, as shown in figure 1, and $\boldsymbol{u} = (u, v, w)$ are the corresponding velocity components. The region $0 \leqslant r \leqslant R(\theta, x, t)$ is occupied by the first liquid with viscosity μ_1 and density ρ_1, and the second liquid with viscosity μ_2 and density ρ_2 is located in $R(\theta, x, t) \leqslant r \leqslant R_2$. The pipe is infinitely long and the mean value of $R(\theta, x, t)$ is R_1, a constant fixed by prescribing the volumes of each liquid, independent of t.

We are interested in the core–annular flow solution of the governing equations:

$$\boldsymbol{U} = (0, 0, W_i(r)), \quad i = 1, 2,$$

$$R(\theta, x, t) = R_1,$$

where R_1 is constant. On the cylindrical interface $r = R_1$,

$$[\![\hat{P}]\!] = T/R_1, \tag{2.1}$$

where T is the interfacial tension and the jump across the interface

$$[\![\cdot]\!] = (\cdot)_1 - (\cdot)_2.$$

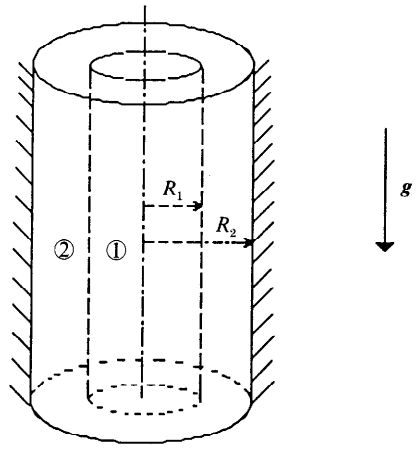

FIGURE 1. Sketch of vertical core–annular flow.

It follows from (2.1) that a necessary condition for the existence of CAF is

$$\frac{\mathrm{d}\hat{P}_1}{\mathrm{d}x} = \frac{\mathrm{d}\hat{P}_2}{\mathrm{d}x} = -f \text{ (constant)}.$$

The axial velocities are

$$W_1(r) = \frac{f+\rho_1 g}{4\mu_1}(R_1^2 - r^2) + \frac{f+\rho_2 g}{4\mu_2}(R_2^2 - R_1^2) + \frac{R_1^2[\![\rho]\!] g}{2\mu_2}\ln\frac{R_2}{R_1}, \quad 0 \leqslant r \leqslant R_1, \quad (2.2a)$$

$$W_2(r) = \frac{f+\rho_2 g}{4\mu_2}(R_2^2 - r^2) - \frac{R_1^2[\![\rho]\!] g}{2\mu_2}\ln\frac{r}{R_2}, \quad R_1 \leqslant r \leqslant R_2. \quad (2.2b)$$

We scale length with R_1, velocity with gR_1^2/ν_1, time with ν_1/gR_1 and pressure with $\rho_1 g^2 R_1^4/\nu_1^2$. The following dimensionless parameters are defined:

$$m = \frac{\mu_2}{\mu_1}, \quad a = \frac{R_2}{R_1}, \quad \zeta_i = \begin{cases} 1, & 0 \leqslant r \leqslant R_1, \quad i = 1, \\ \dfrac{\rho_2}{\rho_1}, & R_1 \leqslant r \leqslant R_2, \quad i = 2, \end{cases}$$

$$\mathbb{R} = \mathbb{R}_1 = \frac{gR_1^3}{\nu_1^2}, \quad \mathbb{R}_2 = \frac{\zeta_2}{m}\mathbb{R}, \quad F = \frac{f}{\rho_1 g},$$

$$J^* = \frac{aTR_1}{\rho_1 \nu_1^2} = \frac{TR_2}{\rho_1 \nu_1^2}.$$

We also introduce $\mathbb{R}_g$

$$\mathbb{R}_g = \frac{R_1(gR_1)^{\frac{1}{2}}}{\nu_1} = \mathbb{R}^{\frac{1}{2}}.$$

The parameter F is the ratio of driving forces, the ratio of the pressure gradient to the force of gravity. The Reynolds number $\mathbb{R}_g$ is based on gravity and is zero in a forced flow when gravity is entirely neglected, a case not considered here. Forced flows with a fixed value of $\mathbb{R}_g$ are characteristic for our experiments. Strong forcing

is then obtained when $|F-1| \gg 1$ for a fixed value of $\mathbb{R}_g$. Free fall without forcing means $F = 0$, the pressure gradient and gravity act in the same direction when the driving force ratio $F > 0$, and in opposition when $F < 0$.

When written in terms of the dimensionless numbers the velocities (2.2) of CAF become

$$W_1(r) = \frac{F+1}{4}(1-r^2)+\frac{F+\zeta_2}{4m}(a^2-1)+\frac{1-\zeta_2}{2m}\ln a, \quad 0 \leqslant r \leqslant 1, \tag{2.3a}$$

$$W_2(r) = \frac{F+\zeta_2}{4m}(a^2-r^2)-\frac{1-\zeta_2}{2m}\ln\frac{r}{a}, \quad 1 \leqslant r \leqslant a. \tag{2.3b}$$

Examination of (2.3a, b) shows that we may determine when the flow goes up and when it goes down with inequalities framed in terms of two values; each one is negative:

$$F_1 = -\frac{\zeta_2(a^2-1)+1}{a^2},$$

$$F_2 = -\frac{m+2\ln a+\zeta_2(a^2-1-2\ln a)}{m+a^2-1}.$$

Three cases are distinguished

down-flow in the core and annulus: $F > F_u$; (2.4)

mixed flow, up in some place, down in another:

$$F_u > F > F_1; \tag{2.5}$$

up-flow in the core and annulus: $F_1 > F$; (2.6)

where $(F_1, F_u) = (F_1, F_2)$ if $\zeta_2 > 1$ and $(F_1, F_u) = (F_2, F_1)$ if $\zeta_2 < 1$.

The situation of interest in pumping against gravity is (2.6) with $F < F_1$ when the water is heavier and outside. Free flow corresponds to downward flow in both core and annulus. The size of the F-interval for which mixed flows are possible is

$$|F_1-F_2| = \frac{|1-\zeta_2|}{a^2-1}\left\{\frac{2a^2\ln a-a^2+1}{a^2}+\frac{m(a^2-1-2\ln a)}{m+a^2-1}\right\}.$$

When the densities are matched $F_1 = F_2$, and mixed flows are not possible.

3. Experiments

We have built two devices to study lubricated vertical core–annular flow. The first set-up is a free-fall apparatus (see figure 2). The fluids are introduced into the pipe in a core and annulus. The entrance for the core is a centrally located stand pipe through which oil is introduced. The water enters through an annulus surrounding the stand pipe. The flow is driven by gravity alone acting on the density difference, care being taken not to introduce large differences in the static heads of oil and water at the entrance. The water and oil are kept separated by the stand pipe wall for a few centimetres before the two streams merge into the test plastic pipe of inner radius 0.3175 cm and 120 cm long. The two fluids empty into the atmosphere simultaneously. We constructed the free-fall apparatus in a rough and ready way solely to demonstrate that a perfect core–annular flow, i.e. the basic flow given by (2.3) with $F = 0$, could be achieved in experiments designed so that the system parameters are

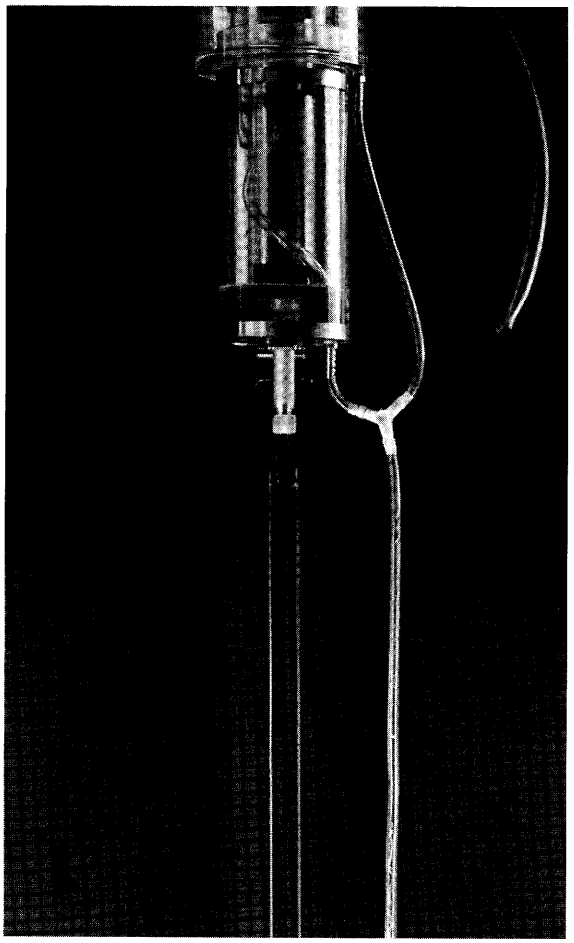

FIGURE 2. Free-fall apparatus. The test section of the pipe is surrounded by a square box filled with glycerine to remove the visual distortion created by the circular pipe. The inner radius of the pipe is 0.3175 cm and the pipe is 120 cm long.

in the window identified as stable by the linear theory. We shall compare theory and experiment in §8.

The second apparatus, shown in figure 5, is a much more carefully designed inverse U loop whose long legs are pipes for up and down flows. These pipes are plastic and are of inner radius 0.48 cm. The second apparatus is used to study forced flows, up when the pressure gradient and gravity are in opposition and down when the pressure and gravity are in the same direction. We are presently collecting data on the flow rates, pressure drops and hold-up ratios for several oil–water systems. We intend to present these data and detailed flow charts following Charles, Govier & Hodgson (1961). We are going to make an extensive and detailed comparison between the linear theory and experiment after we have collected the data we need to input for the theory. We can present a part of these results in this paper, documenting the prediction of perfect CAF in the free fall when the parameters of the experiment are selected in the window of stability. We also present here some representative results for the linear theory to provide the reader with an understanding of the range of phenomena which may be expected from the instabilities of CAF in vertical pipes.

Fluid	Density (gm/cc)	Viscosity (P)	Interfacial tension (dyne/cm)
80%–20% glycerine–water	1.18	0.34	12.27
SAE 30	0.85	1.03	

TABLE 1. Material parameters at 23 °C

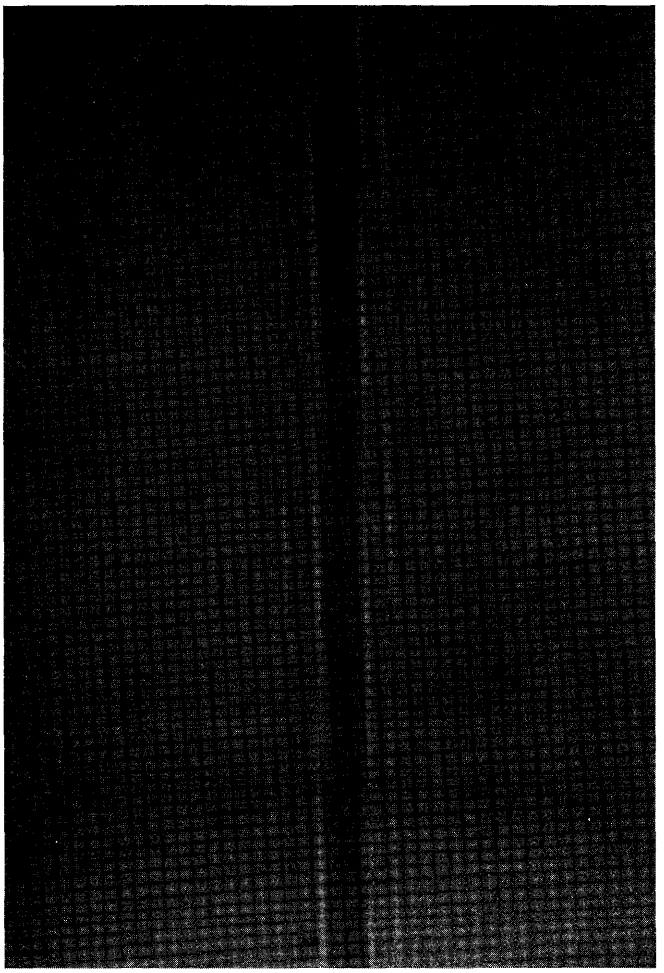

FIGURE 3. Stable perfect core–annular flow of SAE 30 oil and glycerine/water mixture. $a = 1.86$, $m = 0.33$, $\zeta_2 = 1.4$, $J^* = 2.26$, $F = 0$, $\mathbb{R}_g = 1.82$.

3.1. *Free fall*

In free fall there is no pressure gradient, $F = 0$, and the two fluids run down the pipe under the influence of gravity alone. As we shall see later in §8, the linear theory predicts that it is possible to choose parameters so as to achieve a perfect core–annular flow in free fall. It is very important to test this prediction because linearly stable pipe flows of a single fluid are known to be destabilized by finite-amplitude disturbances. The flows which the oil companies call lubricated are wavy core flows, not perfect core–annular flows. At one point we thought that it might be possible that wavy core flows can arise out of a subcritical bifurcation of perfect

core–annular flow. Until we carried out these experiments we had never seen a perfect core–annular flow, though the sketch of experiment 2 by Charles *et al.* (1961) called 'oil in water concentric' is close to perfect and the data for this experiment are nearly in the region of stability (see figure 13 of PCJ). In the experiment reported below, based on the predicted parameters for stable CAF, we built an apparatus and selected fluids to match the prediction and we were successful. Now it is established that it is possible to run a perfect core–annular flow, robustly stable to finite-amplitude disturbances if the operating conditions are stable according to linearized theory.

PCJ have shown that the values of the viscosity ratio m for which stable CAF is possible lie on a bounded, actually not too large interval (see figure 11, PCJ, for example) and there is a certain m, near 0.5, which maximizes the size of the interval of Reynolds numbers for which CAF is stable. From our calculations in §8, we learn that heavy lubricants are beneficial and we can minimize capillary instability by choosing two fluids with a small interfacial tension. We need small interfacial tension, relatively heavy lubricant, a viscosity ratio which is somewhat close to 0.5 and Reynolds number large enough to avoid capillary instability but not too high. These problems were solved by choosing a pipe with inner radius 0.3175 cm, using an 80% glycerine and 20% water (by weight) mixture as the lubricant for the transport of Tropic Artic (Phillip) SAE 30 core fluid (see table 1). With these design parameters we have $\zeta_2 = 1.4$, $m = 0.33$ and we were able to realize stable CAF for various values of a. The example in figure 3 corresponds to $a = 1.86$, $\mathbb{R}_g = 1.82$ and $J^* = 2.66$. The neutral curves for these parameters are exhibited in §8 and it will be shown that the linear theory agrees with experiment. Another stable CAF is shown in figure 4, where the oil has been dyed to improve visual contrast.

We think it is important to draw attention to the effects of the material of construction of the pipe on the problem of lubrication. In fact, it was necessary to thoroughly wash the pipe with glycerine–water mixture. If the pipes were not so prepared we might see flow with oil deposited on the Plexiglas wall. There is an instability which we call 'chugging' which is associated with this failure of lubrication. We really have nothing in our equations to tell us whether the oil or the glycerine–water mixture will be on the wall. This appears to be a problem of adhesion which goes beyond the usual discussions of contact lines.

3.2. *Forced flows*

As explained earlier, we shall only describe some of the qualitative behaviour of forced flow here. A photograph of the U loop we use to study forced flows is shown in figure 5. The working fluids are water and heavy Mobil oil with $\rho = 0.881$ gm/cc, $\mu = 13.32$ P. This gives $\zeta_2 = 1.135$, $m = 0.00067$. Water is introduced in an annulus by small nozzles evenly distributed on a circle on the outer wall of the annulus. The oil is introduced through a thin-walled pipe at the centre of the annulus, and after a few centimetres the flow of the water in the annulus merges with the flow of oil in the pipe. The applied pressure gradient in the water and oil tanks, and the volume flow rates of both water and oil, are adjustable; they are dials with which we control the experiment. We can measure pressure drops and hold-up ratios in the two test sections used to monitor up- and down-flow. The test sections are seen in figure 5 as the portions of the U loop surrounded by boxes filled with glycerine designed to remove the visual distortion which is created by the circular tube. A high-speed video system is used to detect different flow configurations in these boxes and to measure the size of bubbles and slugs and other interesting quantities.

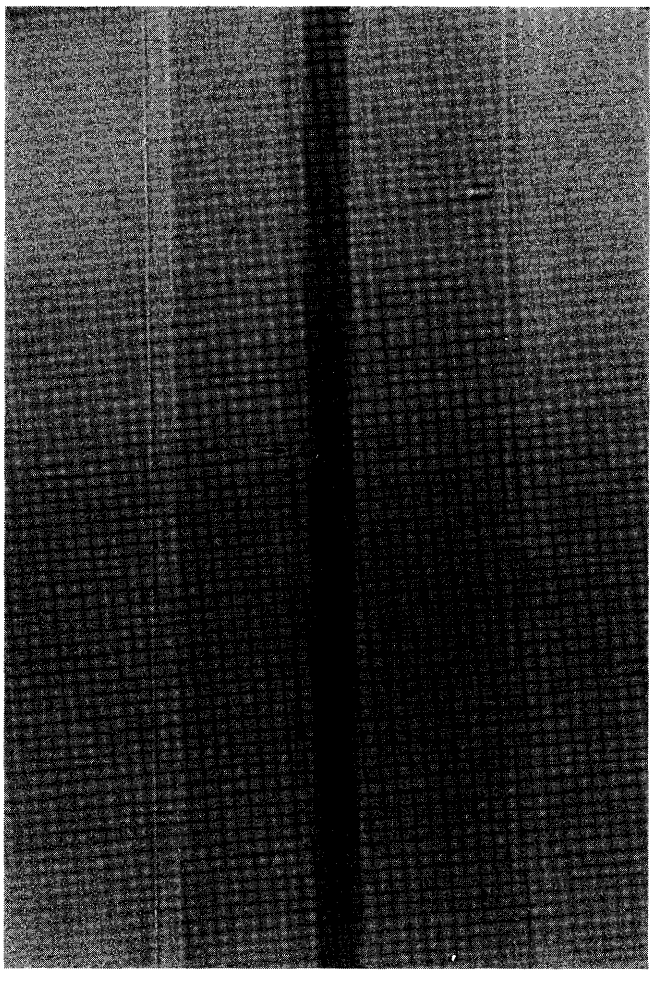

FIGURE 4. Stable perfect core–annular flow of dyed SAE 30 oil and glycerine/water mixture. $a = 1.67$. Material properties of SAE 30 oil and interfacial tension are uncertain due to the addition of dye. The pipe walls are indicated by the arrows.

A sequence of photographs of the flows which are realized as the superficial water velocity $V_w = Q_w/A$ and the superficial oil velocity $V_o = Q_o/A$ are varied is shown in figure 6. Here Q_w, Q_o are the volume flow rates of water and oil respectively and $A = \pi R_2^2$ ($R_2 = 0.48$ cm) is the area of the cross-section of the whole pipe. There are two panels in each photograph: up-flow with the pressure gradient pushing the fluid up against gravity is on the left, down-flow with the pressure gradient pushing the fluid down in the same direction as gravity is on the right. When the oil velocity V_o is small, as in figure 6 (*a*, *b*), oil bubbles are formed both in the up and down flows. These bubbles are a consequence of capillary instability in the unstable left-hand side of the (F, α)-plane of neutral curves shown in §9; for example, figure 21 (*b*). As V_o is increased, wavy core flow is first observed in up-flow on the left, while the down-flow takes the form of bubbles and slugs as in figure 6 (*c*, *d*) or of long slugs as in figure 6 (*e*). This trend can be explained in terms of hold-up ratio, used by Charles *et al.* (1961) in a similar experiment. In general, the input oil–water ratio, $R_{o/w} = Q_o/Q_w$, and the *in situ* ratio, which is the ratio of the volume of the pipe occupied by oil to the volume

FIGURE 5. Forced-flow apparatus. The sections indicated by arrows are test sections and they are surrounded by boxes filled with glycerine to eliminate visual distortion. The left test section is for up-flow and the right is for down-flow. The two extra sections on the far left are only used for demonstration purpose. The inner radius of the pipe is 0.48 cm.

occupied by water, are different because one of the components will tend to accumulate in the pipe. The hold-up ratio, defined as the ratio of the input oil–water ratio to the *in situ* oil–water ratio, is thus an important parameter for core–annular flow. For a given input ratio $R_{o/w}$, if oil accumulates in the pipe the hold-up ratio will be less than unity, and greater than unity if water accumulates in the pipe. When the flow rates are moderate, the accumulation of water in up-flow is greater than in down-flow because the effective gravity accelerates oil (buoyancy) and decelerates water. For down-flow, the opposite is true: gravity decelerates oil and accelerates water. This leads to an accumulation of oil in the down-flow. We have examined the *in situ* ratio in both up and down flows simultaneously and the results confirm that if the flow rates are not too large the *in situ* ratio in the down-flow test section is larger than that in the up-flow test section. At higher speeds this difference is negligible. Mathematically the above statement is equivalent to the statement that for a given input ratio $R_{o/w}$, the parameter a in our analysis has different values for up- and down-flow: a is larger for up-flow than for down-flow. For water and heavy

(a)

(b)

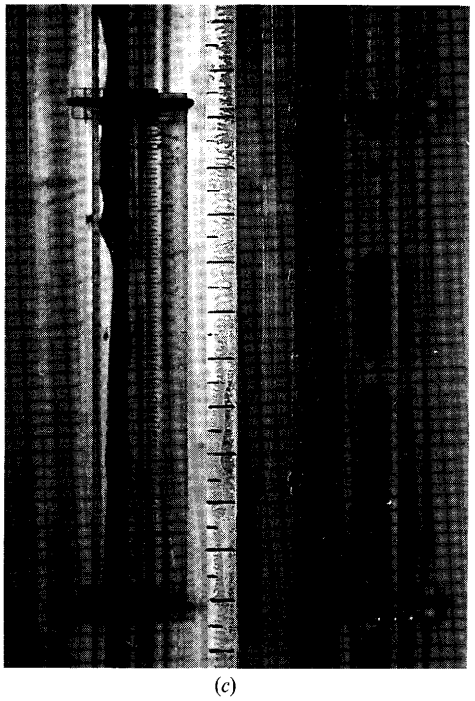

(c)

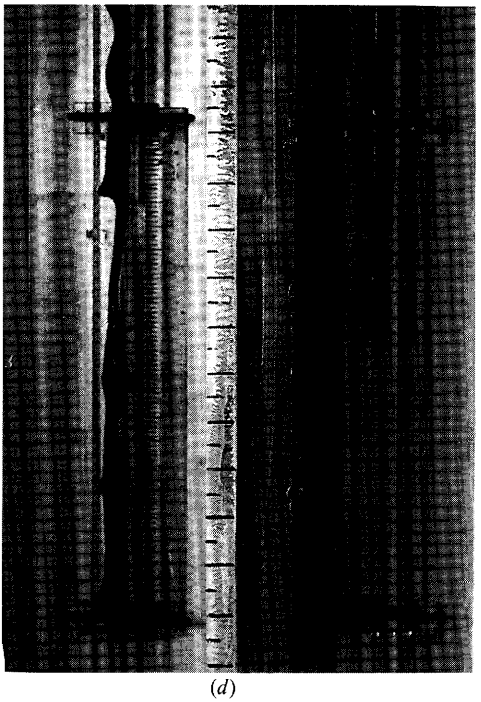

(d)

FIGURE 6(a–d). For caption see p. 262.

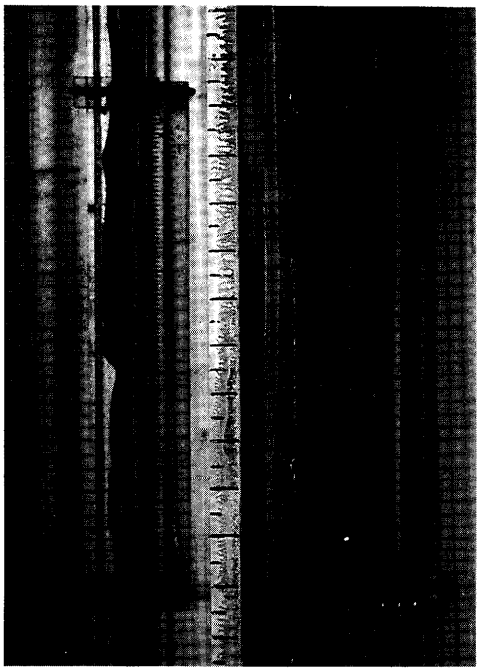

(*e*)

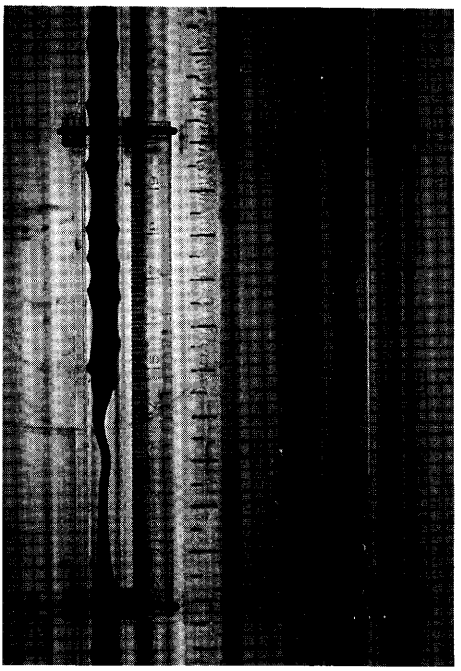

(*f*)

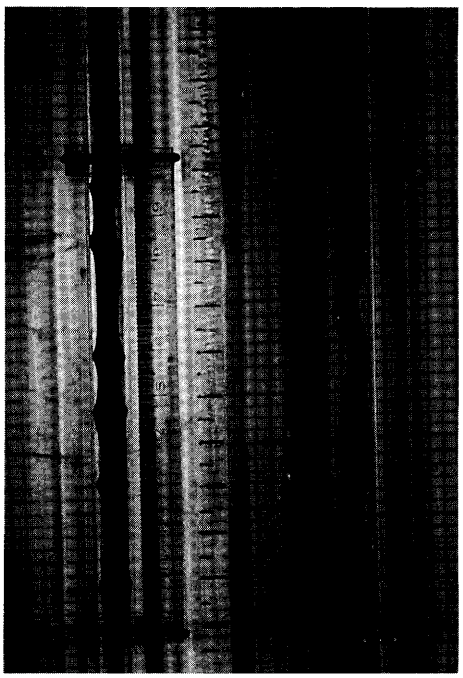

(*g*)

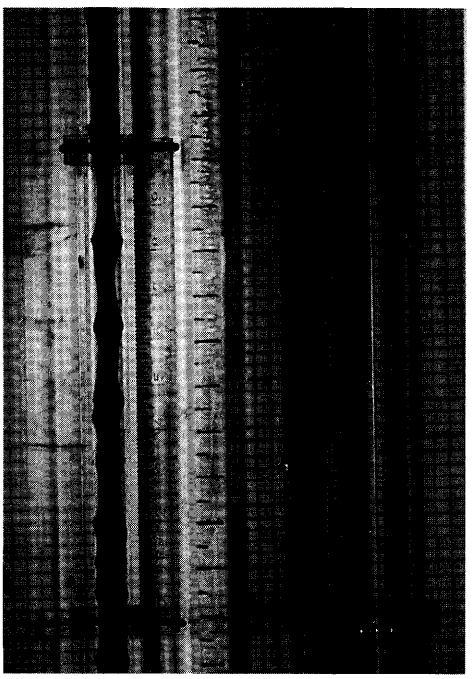

(*h*)

FIGURE 6(*e–h*). For caption see p. 262.

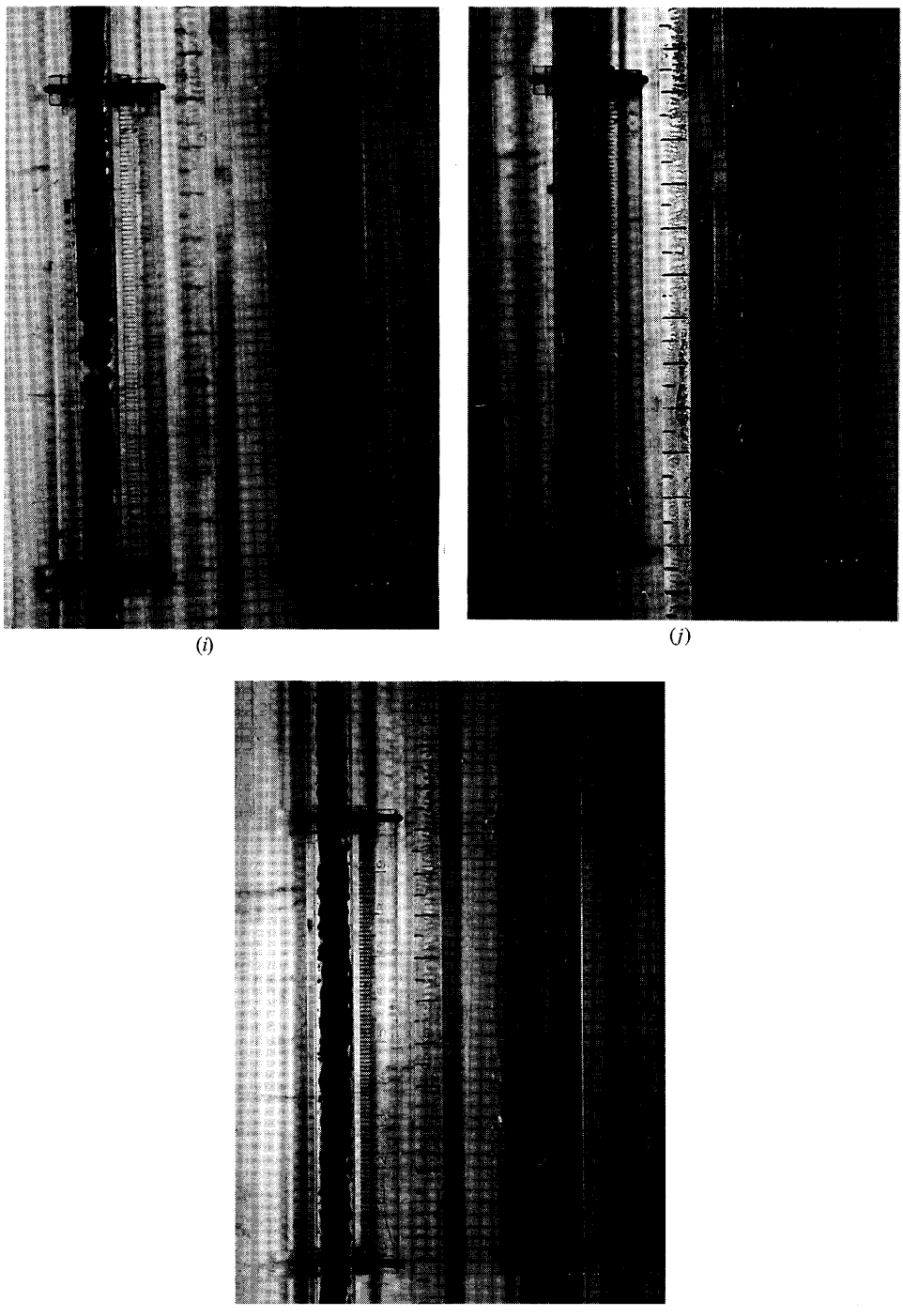

(i) (j) (k)

FIGURE 6. Core–annular flow of heavy Mobil oil and water. The left panel is up-flow, gravity opposes the applied pressure gradient. The right panel is down-flow, gravity aids the applied pressure gradient. V_w and V_o are the superficial velocities of water and oil respectively. (*a*) $(V_w, V_o) = (0.436, 0.283)$ ft/s; (*b*) $(1.56, 0.256)$ ft/s; (*c*) $(0.436, 0.542)$ ft/s; (*d*) $(1.56, 0.582)$ ft/s; (*e*) $(1.56, 0.906)$ ft/s; (*f*) $(0.413, 0.426)$ ft/s; (*g*) $(0.413, 0.426)$ ft/s; (*h*) $(0.554, 0.739)$ ft/s; (*i*) $(0.330, 0.909)$ ft/s; (*j*) $(0.436, 1.766)$ ft/s; (*k*) $(1.116, 1.241)$ ft/s.

Mobil oil, the parameters are not in the window of stable CAF: m is too small, ζ_2 is not large enough, etc. Our discussions in §9 will show that with other parameters fixed, the unstable region will expand as a is increased, typically the upper branch of neutral curves, which is associated with wavy core flows, will sink. The instability on the upper branch is responsible for the wavy flows observed in up-flow while stable slugs occur in down-flow. For faster flows the effects of gravity are small and there is less difference between the up- and down-flows. The differences, which can be observed in figure 6(*f–j*), are again well correlated with the argument about the hold-up ratio which leads to a larger water fraction, less stability, in up-flow.

Many different and interesting nonlinear waves of large amplitude develop in vertical core–annular flow. There is as yet no coherent theory for these waves. We shall make a few casual observations. First, wakes are important, we see the drafting of slugs and bubbles, in which the rear bubble accelerates in the wake of the bubble preceding it, eventually forming a bubble train held together by pressure deficits behind the blunt body. Such trains can be seen at the top of the up-flow panel in figure 6(*a*) and the down-flow panel in figure 6(*d*). This type of wake effect is present also in the wavy core behind the large crests as in the draining of up-flow jets shown in figure 6(*c*), (*d*), (*e*) and (*f*). Large-amplitude axisymmetric waves in up-flow with peaked crests like those shown at the top and the bottom of the left panel of figure 6(*f*) more typically take a corkscrew form in down-flow as is evident in the right panels of figure 6(*f*) and (*g*). It can be argued that all non-axisymmetric waves will be forced to rotate by hydrodynamic couples associated with shear between oil and water.

4. Disturbance equations

The linear stability of CAF can be analysed in the usual way. We introduce the normal modes

$$\begin{bmatrix} u \\ v \\ w \\ p \\ \delta \end{bmatrix} = \begin{bmatrix} \mathrm{i}u(r) \\ v(r) \\ w(r) \\ p(r) \\ \eta \end{bmatrix} \exp\left[\mathrm{i}n\theta + \mathrm{i}\alpha(x-ct)\right],$$

where (u, v, w), p are the perturbed velocity and pressure, and δ is the deviation of the interface from a perfect cylinder of radius one. The spatial mean $\bar{\delta}$ of δ must vanish if the volume of each of the two fluids is conserved in the linear approximation. The equations governing disturbance amplitudes are the same as those of (5.3), (5.4), (5.5) in PCJ except that the basic flow is given by (2.3).

The form of boundary conditions and centreline conditions are the same as (5.6), (5.15) in PCJ. The interfacial conditions, (5.7), (5.8), (5.10) and (5.11) in PCJ are unchanged, but (5.9) which arises from the balance of shear tractions has to be replaced by

$$\left[\!\left[\frac{\zeta}{\mathbb{R}} W''(1)\right]\!\right] u(1) + \left[\!\left[\frac{\zeta}{\mathbb{R}}(w'-\alpha u)\right]\!\right] \alpha(W(1)-c) = 0. \tag{4.1}$$

This change is solely due to the presence of the density difference because

$$\left[\!\left[\frac{\zeta}{\mathbb{R}} W''(1)\right]\!\right] = \frac{\zeta_2 - 1}{\mathbb{R}}. \tag{4.2}$$

The condition (4.1) is better understood when written in dimensional form. It arises originally from the statement that the shear stress τ_{rx} is continuous across the interface $r = R_1 + \delta$:

$$(1-\delta_x^2)[\![\mu(W'(r)+w_r+u_x)]\!]+2\delta_x[\![\mu(u_r-w_x)]\!]=0. \tag{4.3}$$

The continuity of the shear stress for the basic flow for $\delta = 0$ is in the form

$$[\![\mu W'(R_1)]\!]=0 \tag{4.4}$$

and

$$[\![\mu W''(R_1)]\!]=-[\![\rho]\!]g. \tag{4.5}$$

To leading order (4.3) reduces to

$$[\![\mu W''(R_1)]\!]\delta+[\![\mu(w_r+u_x)]\!]=0. \tag{4.6}$$

This shows that the jump in the shear stress on $r = R_1$ is balanced by the effective gravity

$$[\![\rho]\!]g\delta=[\![\mu(w_r+u_x)]\!]. \tag{4.7}$$

The instability associated with (4.7) is induced by gravity. The only stable equilibrium of two fluids in gravitational field is vertically stratified. Hence, when the velocity is reduced to zero the heavy fluid will fall into a stratified configuration with heavy fluid below. Experiments (cf. §3) and analysis show that this fall-down instability can be stabilized by shear. The gravity term in this system of equations is not conservative because

$$\operatorname{curl}\rho\boldsymbol{g}=\boldsymbol{g}\wedge\nabla\rho\neq 0 \tag{4.8}$$

where $\nabla\rho$ is distributional across the interface.

HJ showed that the linearized energy equation may be used to identify sources of instabilities. The new features of the energy equation are the extra terms arising from the interface. Each of these terms is proportional to one of the material jumps of the two fluids. The growth rate of the energy of small disturbances is given by

where

$$\mathring{E}=I-D+B, \tag{4.9}$$

$$\left.\begin{aligned}
&\mathring{E}=\alpha c_{\mathrm{i}}\int_\Omega \zeta_j r(u^2+v^2+w^2)\,\mathrm{d}r,\\
&I=\int_\Omega \zeta_j r W_j'(r)\,\mathrm{Im}\,(uw^*)\,\mathrm{d}r,\\
&D=\int_\Omega \frac{\zeta_j}{\mathbb{R}_j}\left\{\frac{1}{r}\left(\frac{\mathrm{d}ru}{\mathrm{d}r}\right)^2+\frac{1}{r}\left(\frac{\mathrm{d}rv}{\mathrm{d}r}\right)^2+r\left(\frac{\mathrm{d}w}{\mathrm{d}r}\right)^2\right.\\
&\qquad\left.+r\left(\alpha^2+\frac{n^2}{r^2}\right)(u^2+v^2+w^2)+\frac{4n}{r}\,\mathrm{Re}\,(u^*v)\right\}\mathrm{d}r+\frac{1}{\mathbb{R}}(u^2(0)+v^2(0)),\\
&B=B1+B2+B3,\\
&B1=\frac{J^*}{\alpha\mathbb{R}^2}\frac{1-\alpha^2-n^2}{\alpha}\frac{c_{\mathrm{i}}}{|W(1)-c|^2}u^2(1),\\
&B2=\frac{1-m}{\mathbb{R}}\left\{2(u^2+v^2)+2\alpha\,\mathrm{Re}\,(u^*w_2)+2n\,\mathrm{Re}\,(uv^*)\right.\\
&\qquad\left.-\frac{F+1}{2}\frac{1}{\alpha}\mathrm{Re}\left(\frac{u^*w_2'}{(W(1)-c)^*}\right)-\frac{F+1}{2m}\frac{(2-m)(W(1)-c_{\mathrm{r}})}{|W(1)-c|^2}u^2(1)\right\},\\
&B3=-(\zeta_2-1)\frac{1}{\alpha}\mathrm{Re}\left(\frac{uw_2^*}{W(1)-c}\right)+\frac{1-m}{\mathbb{R}}\frac{F+1}{\alpha^2|W(1)-c|^2}\frac{\zeta_2-1}{2m}u^2(1).
\end{aligned}\right\} \tag{4.10}$$

and

$$c_r = \mathrm{Re}\,(c), \quad c_i = \mathrm{Im}\,(c) > 0, \quad \text{for instability},$$

where Re stands for real part, Im for imaginary part,

$$\int_\Omega (\cdot)\,\mathrm{d}r = \int_0^1 (\cdot)_1\,\mathrm{d}r + \int_1^a (\cdot)_2\,\mathrm{d}r,$$

and an asterisk denotes the complex conjugate.

Here, $\mathring{E}$ is the rate of change of kinetic energy of the perturbed flow; I is the rate at which energy is transferred from the basic flow to the perturbed flow through Reynolds stress; $-D$ is the rate of viscous dissipation of the perturbed flow and B is the rate at which the energy is being supplied at the interface. $\mathring{E}$ and D may be further decomposed into a part in the water and a part in the oil. It is clear that $B1$ is the energy supplied at the interface due to interfacial tension. It originates from the normal stress balance at the interface and arises from a perturbation of the curvature of the interface. Interfacial tension stabilizes short waves and all asymmetric waves ($n \geqslant 1$), and destabilizes long axisymmetric waves.

$B2$ is the energy supply due to the viscosity jump which HJ called 'interfacial friction'. It comes from perturbing the condition expressing the continuity of velocity. This leads to a jump in the shear rate which can be reduced to a viscosity jump. Instability due to interfacial friction is a viscous generalization of the Kelvin–Helmholtz instability. It has been found that when the densities are matched $B2$ stabilizes the flow at low Reynolds numbers, destabilizes at high Reynolds numbers and causes wavy core flows. The term $B3$ in the energy supply is proportional to the jump of the density, with gravity as a constant of proportionality. We have used gR_1^2/ν_1 as the velocity scale so that the gravity effect is implicit. The last term in $B3$ also contains a factor proportional to the viscosity difference, indicating the coupling of the effect of the viscosity jump and the effect of the density jump. We call $B3$ interfacial gravity.

It is clear from the energy equation that even when viscosities are matched ($m = 1$) and $J^* = 0$, there is still an interfacial energy supply $B = B3$ due to interfacial gravity which can induce instability.

5. Numerical method

Following PCJ we applied a Chebyshev pseudo-spectral method to our eigenvalue problem. After introducing domain mappings and interpolation functions, as in PCJ, we obtain a discrete system of equations expressed in terms of nodal values in the following form

$$(\boldsymbol{A} + c\boldsymbol{B})\,\boldsymbol{x} = 0.$$

This algebraic eigenvalue problem is then solved by the IMSL routine EIGZC on Cyber205.

Convergence tests performed by increasing the truncation number N of the interpolation functions are shown in table 2. These tests confirm the property of exponential convergence of the pseudo-spectral Chebyshev method and demonstrate high accuracy with $N = 20$, which was used in our code. Our code is a modification of the one used by PCJ which was checked against JRR and double checked by HJ. If we take $\zeta_2 = 1$ and

$$F = \frac{4m}{m + a^2 - 1} - 1,$$

N	$\alpha = 0.2$	$\alpha = 0.4$
14	(3.737404964933 4, −0.205811112884 2)	(7.319648018537 6, −0.523218316177 5)
	(12.323064298926, −2.711650786734 2)	(25.706130236950, −3.946973327401 9)
	(12.060966954248, −2.887849569403 8)	(25.759034733466, −4.116637279930 1)
20	(3.739993735155 1, −0.204673988881 4)	(7.320932765391 9, −0.522415504441 8)
	(12.323020570 444, −2.711477162723 6)	(25.706135783997, −3.947002811386 2)
	(12.060966966151, −2.887849567568 6)	(25.759034733926, −4.116637272473 6)
25	(3.739982183448 2, −0.204672981904 1)	(7.320923830298 8, −0.522407029306 9)
	(12.323023006793, −2.711482453633 7)	(25.706136187752, −3.946996576231 2)
	(12.060965379790, −2.887847701230)	(25.759040274883, −4.116645913823 1)

TABLE 2. Convergence tests for the three least stable modes. $a = 1.1$, $m = 0.5$, $\zeta_2 = 2.0$, $J^* = 2000$, $\mathbb{R}_g = 10$, $F = 20$

then our problem is identical with that of PCJ. Using this relation, we have again checked the consistency of our code with the one used by PCJ.

PCJ showed that the axisymmetric modes are the most dangerous when gravity is neglected. This result appears to carry over to all the different cases studied in the present problem. We have computed the growth rates for both axisymmetric and asymmetric modes $n = 1$ and 5 for $a = 1.1$, $m = 0.95$, $\zeta_2 = 0.2$, $J^* = F = 0$, $\mathbb{R}_g = 10$, which is a free flow under gravity. The axisymmetric mode $n = 0$ has the largest growth rate. Similar mode comparisons have been carried out for other ranges of parameters and we found that the axisymmetric mode was always most unstable. The axisymmetric and $n = 1$ mode were compared for the upward flow against gravity. The axisymmetric mode was again the most dangerous. In the rest of this paper, we restrict our attention to axisymmetric disturbances.

6. Density stratification and interfacial gravity

Interfacial gravity plays an important role in the disturbance energy budget. Density stratification could either stabilize or destabilize the basic flow, depending on the parameters. To illustrate the effect of density stratification, we consider the following two examples.

In the first example, we have calculated the growth rates for $a = 1.1$, $m = 1$, $J^* = F = 0$, $\mathbb{R}_g = 10$, corresponding to free fall with matched viscosities and zero interfacial tension. Figure 7 shows that the flow is stable when the lubricant is heavier than the core fluid and unstable when lighter. The interfacial mode degenerates to the neutral mode $c = W(1)$ when the densities are also matched. This example indicates that density stratification could cause instability even in the absence of interfacial tension and interfacial friction.

We next consider the lubricated case, $m = 0.5$. JRR showed that for a horizontal pipe with matched density, in the absence of interfacial tension, CAF is stable to long waves if the lubricating layer is very thin. But if the lubricating layer is thick, CAF is unstable to long waves, even in the limit $\mathbb{R} \to 0$. This long-wave instability is due to interfacial friction. Interfacial tension can also induce a long-wave instability. For the vertical pipe flow studied here, say free fall, the same type of long-wave instability due to interfacial friction will be present if the radius ratio a is large, the densities are matched and interfacial tension is neglected. We want to determine if this long-wave instability can be stabilized by density stratification. We have

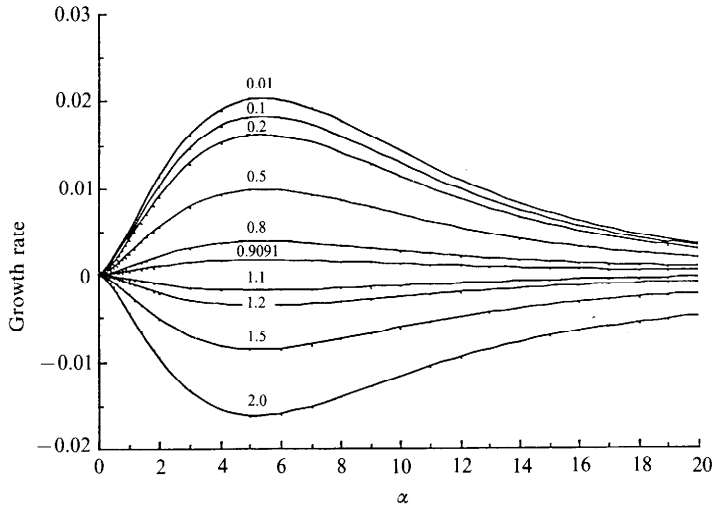

FIGURE 7. Growth rates for $a = 1.1$, $m = 1$, $J^* = F = 0$, $\mathbb{R}_g = 10$, and various values of ζ_2 indicated above each curve. The flow is stable when $\zeta_2 > 1$ and unstable when $\zeta_2 < 1$.

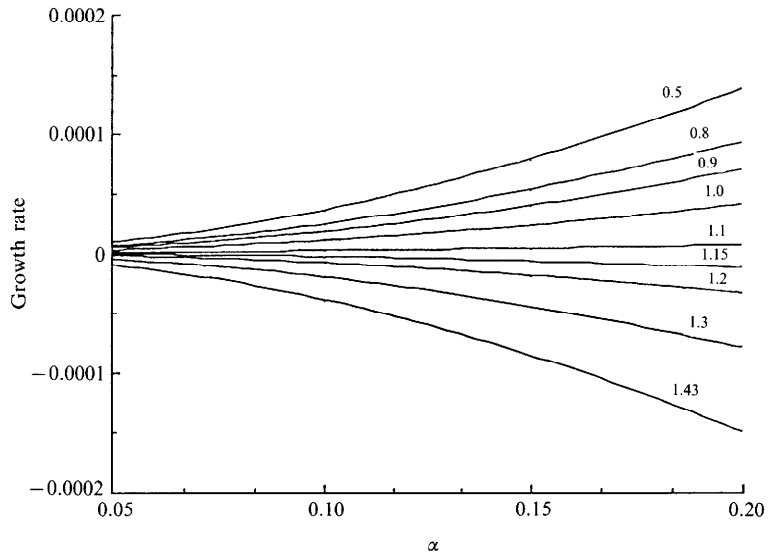

FIGURE 8. Growth rates for $a = 1.86$, $m = 0.5$, $J^* = F = 0$, $\mathbb{R} = 1$, and various values of ζ_2 indicated above each curve. The JRR long-wave instability ($\zeta_2 = 1$) is reinforced when $\zeta_2 < 1$, suppressed when $\zeta_2 > 1$ and stabilized when $\zeta_2 \geqslant 1.15$.

computed the case $a = 1.86$, $m = 0.5$, $J^* = F = 0$, $\mathbb{R}_g = 1$, and various values of density ratio ζ_2, for the long waves $\alpha \ll 1$. The results are shown as plots of growth rates αc_i *vs.* ζ_2 in figure 8. From these plots it is clear that the JRR long-wave instability ($\zeta_2 = 1$) is reinforced when $\zeta_2 < 1$, suppressed when $\zeta_2 > 1$ and completely stabilized when $\zeta_2 > \zeta_J (> 1)$. In our case, ζ_J is about 1.15.

The stabilizing effect of using heavy lubricant seems to work generally. When interfacial tension is included, short waves ($\alpha > 1$) are stabilized and there is a battle in the long-wave range $0 < \alpha < 1$ between the destabilizing effect of surface tension and stabilizing effect of density stratification. In the rest of this section, we shall include interfacial tension and monitor the terms in the energy budget corresponding

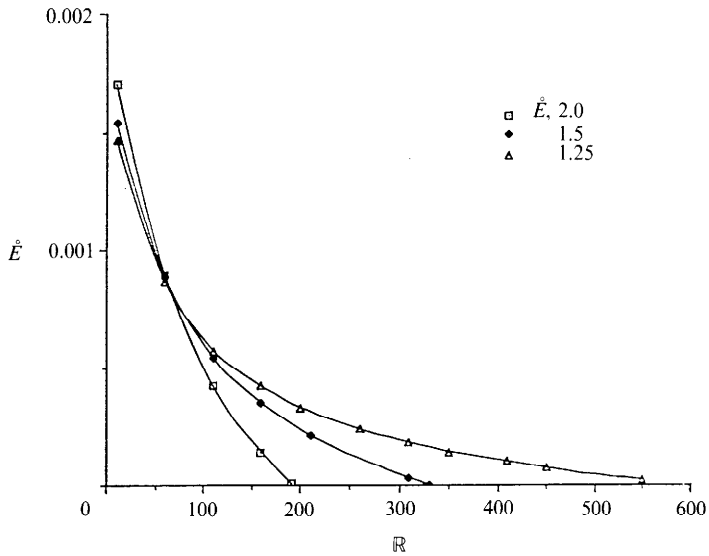

FIGURE 9. The rate of change of disturbance energy $\mathring{E}$ *vs.* Reynolds number $\mathbb{R}$ for $a = 1.1$, $m = 1$, $F = 0$, $J^* = 2000$, $\zeta_2 = 2.0$, 1.5, 1.25. The flow is stable when $\mathbb{R} > \mathbb{R}_c(\zeta_2)$: $\mathbb{R}_c(2.0) = 190$, $\mathbb{R}_c(1.5) = 330$, $\mathbb{R}_c(1.25) = 550$.

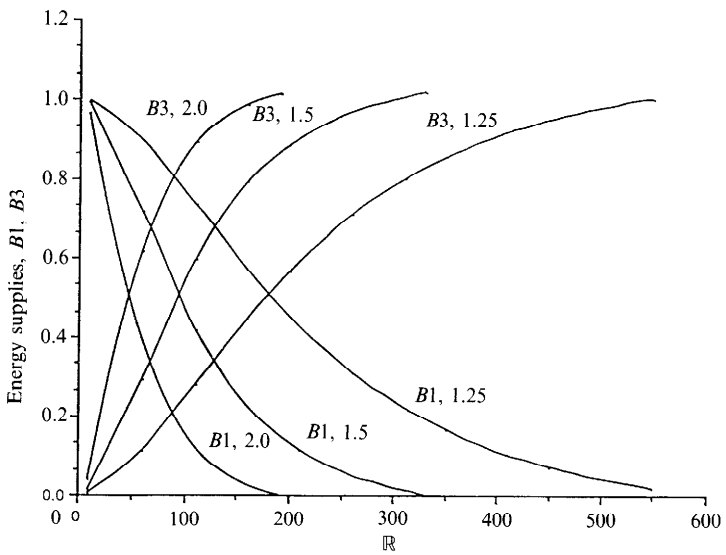

FIGURE 10. Energy supply $B1$, $B3$ for $a = 1.1$, $m = 1$, $F = 0$, $J^* = 2000$, $\zeta_2 = 2.0$, 1.5, 1.25. Interfacial gravity $B3$ is always positive, destabilizing the flow.

to the most unstable mode as the Reynolds number is varied. In performing such calculations, we shall normalize our eigenfunction with $D = 1$. We choose the following parameters: $a = 1.1$, $J^* = 2000$, $F = 0$, $m = 1$ and various values of ζ_2, as one example of free flow under gravity. By matching the viscosities we make the $B2$ term in the energy budget vanish so that we can isolate and study the interfacial gravity $B3$.

We start with $\zeta_2 > 1$, the heavy fluid is outside. In figure 9, the rate of change of the disturbance energy $\mathring{E}$ is plotted against Reynolds number $\mathbb{R}$ for three different

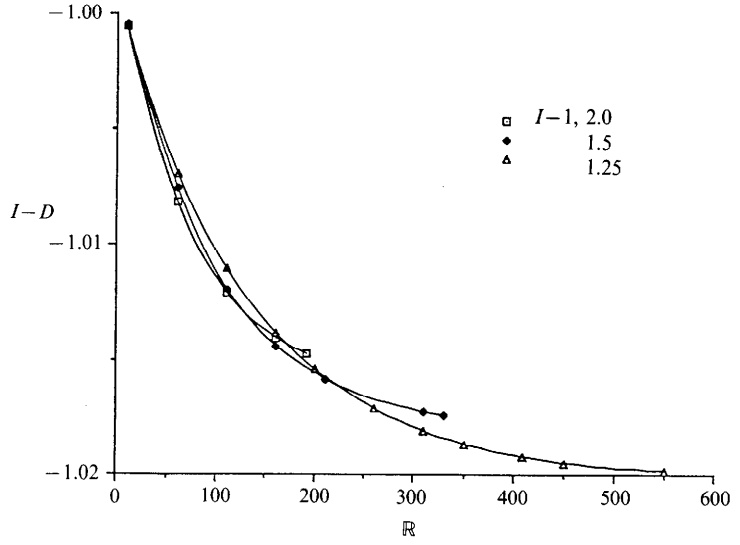

FIGURE 11. $I-D$ for $a = 1.1$, $m = 1$, $F = 0$, $J^* = 2000$, $\zeta_2 = 2.0, 1.5, 1.25$.

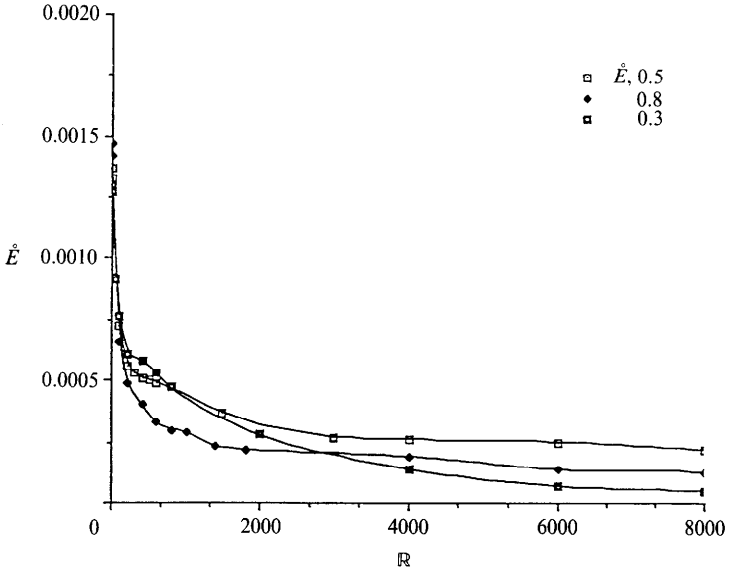

FIGURE 12. Rate of change of disturbance energy $\mathring{E}$ for $a = 1.1$, $m = 1$, $F = 0$, $J^* = 2000$ and $\zeta_2 = 0.8, 0.5, 0.3$. The flow is always unstable.

values of ζ_2. As $\mathbb{R}$ is increased to $\mathbb{R}_c(\zeta_2)$, $\mathring{E}$ monotonically decays to zero. The flow is stable when $\mathbb{R} > \mathbb{R}_c(\zeta_2)$. The fact that $\mathbb{R}_c(2.0) < \mathbb{R}_c(1.5) < \mathbb{R}_c(1.25)$ indicates that increasing the density of the lubricating fluid can stabilize the flow. Water is a good lubricant for oil. Glycerine may be even better. This point can be more clearly seen from figure 10, where we compare the interfacial energy supply $B1$. Capillary instability is rapidly stabilized by using heavy lubricant. This result could be used for preventing the formation of slugs and bubbles in slow flows.

Figure 10 also shows that interfacial gravity $B3$ is always positive and destabilizes the flow. In fact $B3$ is a monotonically increasing function of $\mathbb{R}$ and levels off at large $\mathbb{R}$. Although the interfacial gravity is always destabilizing, the flow is stable when

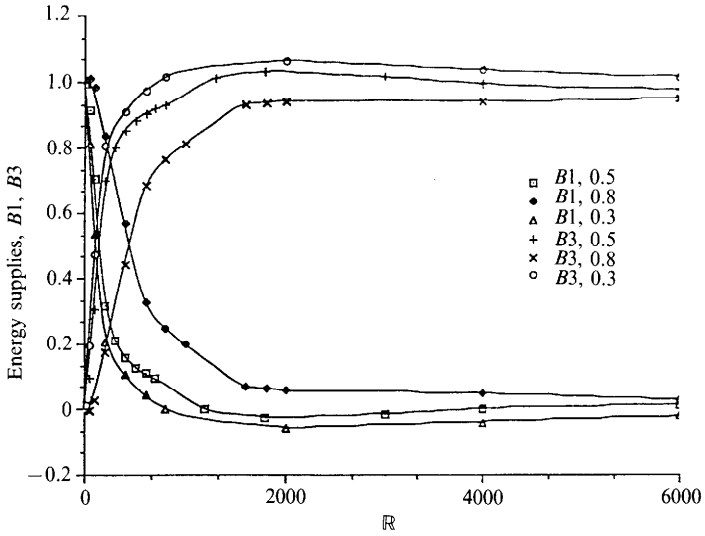

FIGURE 13. Energy supply $B1$, $B3$ for $a = 1.1$, $m = 1$, $F = 0$, $J^* = 2000$ and $\zeta_2 = 0.8, 0.5, 0.3$. At large Reynolds numbers, interfacial gravity $B3$ is the main source of instability.

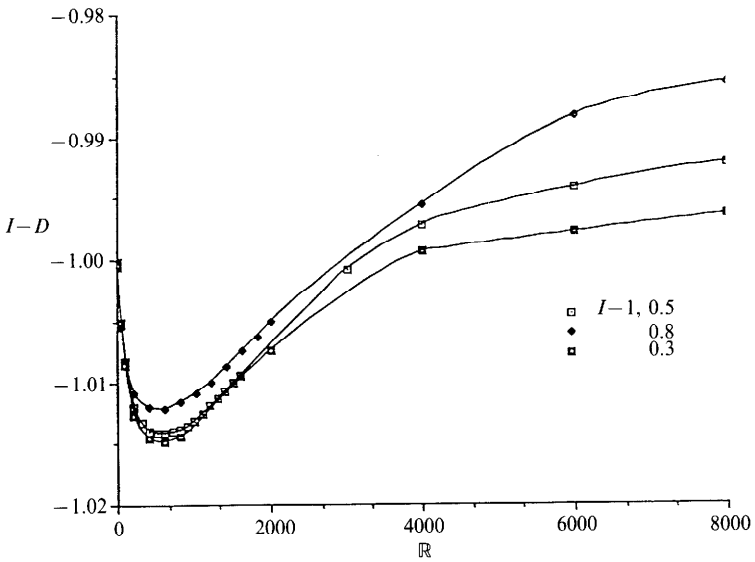

FIGURE 14. $I-D$ for $a = 1.1$, $m = 1$, $F = 0$, $J^* = 2000$ and $\zeta_2 = 0.8, 0.5, 0.3$.

$\mathbb{R} > \mathbb{R}_c(\zeta_2)$. The larger ζ_2, the faster $B1$ decays and the faster $B3$ increases. The Reynolds stress $I-D$ in the bulk fluids is plotted in figure 11. It is always stabilizing. This result indicates that the stabilizing effect of using heavy lubricant is achieved through increasing viscous dissipation, not through interfacial gravity $B3$.

When $\zeta_2 < 1$, the heavy fluid is in the core and the results are very different. The density stratification helps instability and the flow is always unstable for all the Reynolds numbers we have computed. Figure 12 shows that the rate of change of the disturbance energies $\mathring{E}$ for $\zeta_2 = 0.8, 0.5, 0.3$ are positive and monotonic decreasing functions of Reynolds number. In figure 13, we have plotted the energy supply $B1$ and interfacial gravity $B3$ against Reynolds number. At low Reynolds numbers,

interfacial tension is the main source of instability and at large Reynolds numbers the interfacial gravity is the main source of instability. The smaller the value of ζ_2, the faster this transition of type of instability occurs.

Figure 14 shows that $I-D$ is stabilizing for all Reynolds numbers. The following conclusions can be drawn for flows falling freely under gravity, $F = 0$:

(1) Heavy lubricant suppresses the long-wave instability caused by interfacial tension and prevents the formation of slugs and bubbles.

(2) Heavy lubricants can also stabilize the JRR long-wave instability due to interfacial friction which occurs when a is large.

(3) Capillary instability is dominant at low Reynolds numbers and is stabilized by shear at large Reynolds numbers.

(4) Interfacial gravity is always destabilizing and increasingly so at higher Reynolds numbers. When the viscosities are matched and the lubricant is lighter, interfacial gravity is responsible for instability at large Reynolds numbers.

7. Long waves

In the long-wave limit $\alpha \to 0$, the eigenvalue problem can be solved explicitly with a series of powers of α using the method of Yih (1967). The solution was first given by Hickox (1971), in terms of a different set of parameters than ours. The surface tension parameter used by Hickox is

$$S = \frac{T}{\rho_1 R_1 W_1^2(0)},$$

where $W_1(0)$ is the centreline velocity. As pointed out by PCJ, S is not a good surface tension parameter for the study of core–annular flow, since it depends strongly on the velocity. We prefer surface tension parameter J^*, defined in §2, which was first introduced by Chandrasekhar (1961) in his study of capillary instability of jets of viscous liquid in air.

The formula thus obtained for the eigenvalue c can be written as

$$c = c^{(0)} + \alpha c^{(1)} + O(\alpha^2), \tag{7.1}$$

where $c^{(0)}$ is a real constant and thus does not affect stability and $c^{(1)}$ is purely imaginary and therefore determines the stability at the lowest order. In fact $c^{(1)}$ can be written as

$$c^{(1)} = \mathrm{i}\left\{\frac{J^*}{\mathbb{R}} f_1(a, m) + \mathbb{R} f_2(a, m, \zeta_2, F)\right\}, \tag{7.2}$$

where $f_1(a, m)$ is definite positive, measuring the capillary instability modified by shearing. The function $f_2(a, m, \zeta_2, F)$ indicates the effects of interfacial shearing and interfacial gravity on the long-wave stability, since $f_2(a, m, \zeta_2, F)$ can be expressed as

$$f_2(a, m, \zeta_2, F) = (1-m)\, q_1(a, m, \zeta_2, F) + (1-\zeta_2)\, q_2(a, m, \zeta_2, F). \tag{7.3}$$

We also noted that $f_2(a, m, \zeta_2, F)$ is a quadratic polynomial in ζ_2. The details of these functions are given in the Appendix.

Consider free flow under gravity ($F = 0$). If $f_2(a, m, \zeta_2, 0)$ is negative, then there exists a critical Reynolds number $\mathbb{R}_0$, defined in the same way as $\mathbb{R}_g$ in §2, determined by

$$\frac{\mathbb{R}_0^4}{J^*} = -\frac{f_1(a, m)}{f_2(a, m, \zeta_2, 0)}, \tag{7.4}$$

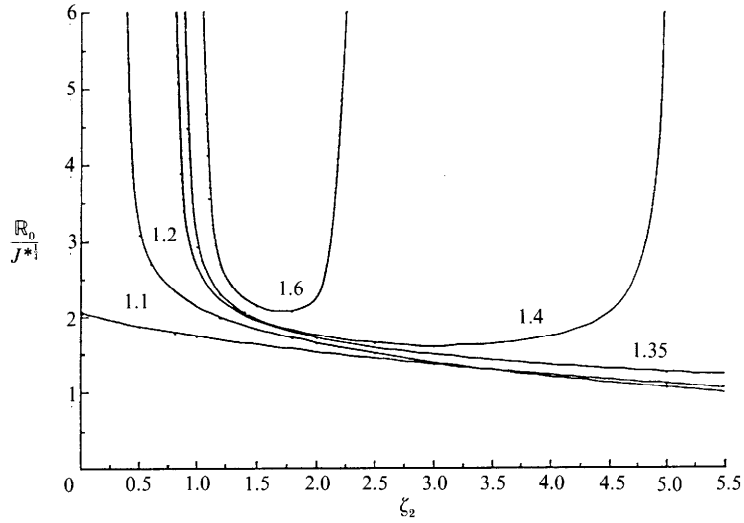

FIGURE 15. Critical $\mathbb{R}_0/J^{*\frac{1}{4}}$ *vs.* ζ_2 for $\alpha = 0$, $m = 0.5$, $F = 0$, and a as a parameter with value given above each curve.

such that we have stability to long waves when $\mathbb{R}_g > \mathbb{R}_0$ and instability when $\mathbb{R}_g < \mathbb{R}_0$. Shear stabilizes capillary instability when $\mathbb{R}_g > \mathbb{R}_0$ (PCJ; HJ).

In figure 15, we have plotted $\mathbb{R}_0/J^{*\frac{1}{4}}$ *vs.* ζ_2 for $m = 0.5$ and different values of a. As we mentioned earlier, the function $f_2(a, m, \zeta_2, F)$ is a parabola on the (f_2, ζ_2)-plane for any given value of a, m and F and $f_1(a, m)$ is a constant for given a, m. For the parameters we choose, f_2 is a concave-up parabola. For the ζ_2 range of interest, say $0 < \zeta_2 < 5.5$, there are three distinct cases, depending on the values of a:

(1) For small a (say $a = 1.1$) there is a region of stability $\mathbb{R}_g > \mathbb{R}_0(\zeta_2)$, for all $0 < \zeta_2 < 5.5$.

(2) $\mathbb{R}_0(\zeta_2) \to \infty$ as $\zeta_2 \to \zeta_0$. There is one and only one ζ_0 in this range. This ζ_0 is one of the two zeros of the parabola $f_2(a, m, \zeta_0, 0)$, falling in the ζ_2 range considered. An example of this is the curve for $a = 1.2$. When $\zeta_2 < \zeta_0$, the flow is unstable to long waves at every $\mathbb{R}_g > \mathbb{R}_0 = 0$; when $\zeta_2 > \zeta_0$ and $\mathbb{R}_g > \mathbb{R}_0$ the flow is stable to long waves, when $\zeta_2 > \zeta_0$ and $\mathbb{R}_g < \mathbb{R}_0$ the flow is unstable to long waves.

(3) There are two critical density ratios ζ_{01} and ζ_{02}, $\mathbb{R}_0(\zeta_2) \to \infty$ as $\zeta_2 \to \zeta_{01}$ or ζ_{02}. The ratios ζ_{01} and ζ_{02} are the two zeros of $f_2(a, m, \zeta_2, 0)$ and they are both in the range $0 < \zeta_2 < 5.5$. The flow is unstable to long waves when $\zeta_{01} < \zeta_2 < \zeta_{02}$ at all $\mathbb{R}_g < \mathbb{R}_0(\zeta_2)$ and is stable when $\mathbb{R}_g > \mathbb{R}_0$. When $\zeta_2 < \zeta_{02}$ or $\zeta_2 > \zeta_{02}$ the flow is unstable at all values of $\mathbb{R}_0$. The curves for $a = 1.4$ and 1.6 are of this type.

The above classifications only make sense in the range of ζ_2 considered, i.e. $0 < \zeta_2 < 5.5$ In fact type (3) is the generic case. But for smaller values of a, one or both of the zeros ζ_{01} and ζ_{02} of $f_2(a, m, \zeta_2, 0)$ may be either negative or too large out of the range of interest.

For forced flow $F \neq 0$, we can determine $\hat{F}_u$ and $\hat{F}_l$ for given values of $\mathbb{R}_g$ and the other parameters such that when $\hat{F}_l < F < \hat{F}_u$, long waves are unstable. This corresponds to capillary instability. Some examples are given in §9.

It was shown by PCJ and Renardy (1987) that maximum growth rates occur when the wave numbers are of order 1 rather than for long waves ($\alpha \to 0$). It is therefore never sufficient to discuss the stability of CAF to long waves alone.

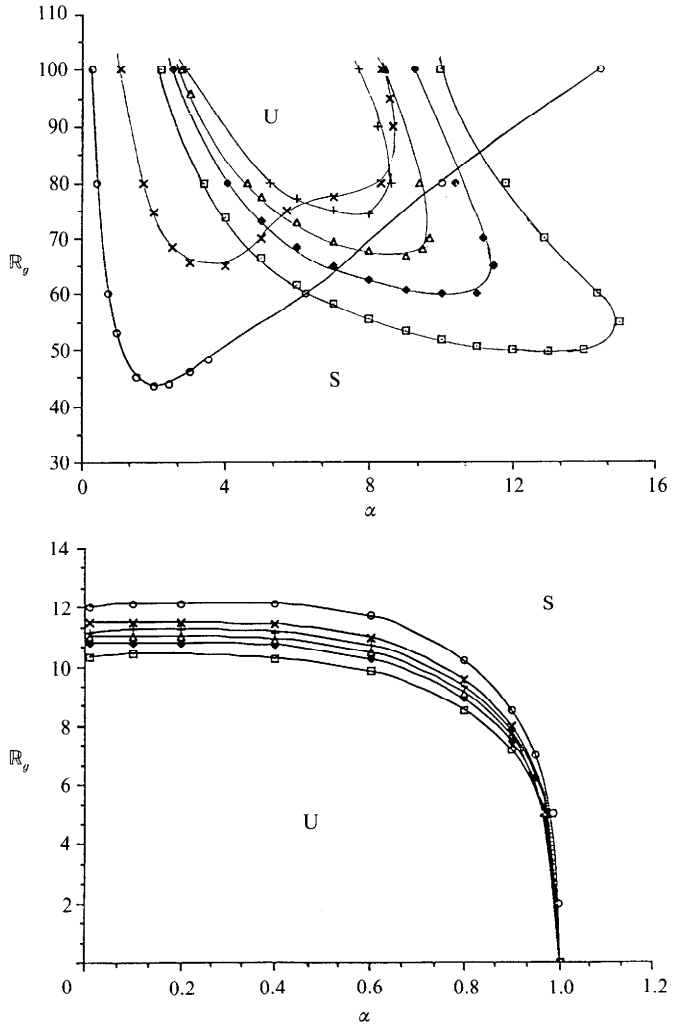

FIGURE 16. Lower and upper branches of the neutral curves for $a = 1.1$, $m = 0.5$, $F = 0$, $J^* = 2000$, $\zeta_2 = 2.0, 1.6, 1.4, 1.2, 1.0, 0.5$. Stable and unstable regions are marked by S and U respectively. The plotting symbols for ζ_2 are: ⊡, 2.0; ◆, 1.6; △, 1.4; +, 1.2; ×, 1.0; ○, 0.5.

8. Neutral curves: free-fall flow under gravity

The simplest vertical CAF is free fall under gravity, $F = 0$. This flow can be realized physically by slowly pouring fluids into a vertical pipe (cf. §3.1). The effects of density stratification in free fall can be determined by comparing neutral curves in the $(\mathbb{R}_g, \alpha)$-plane.

In figures 16–19, we have generated neutral curves for $a = 1.1$, 1.2, 1.3, $m = 0.5$, $J^* = 2000$, and $\zeta_2 = 0.5$, 1.0, 1.2, 1.4, 1.6, 2.0.

The following observations can be obtained from inspecting the neutral curves for $a = 1.1$:

(1) There is an interval

$$\mathbb{R}_L < \mathbb{R}_g < \mathbb{R}_U \tag{8.1}$$

in which CAF is stable for all the six values of ζ_2. Here $\mathbb{R}_L$, $\mathbb{R}_U$ are the maximum and minimum Reynolds numbers on the lower and upper branch respectively.

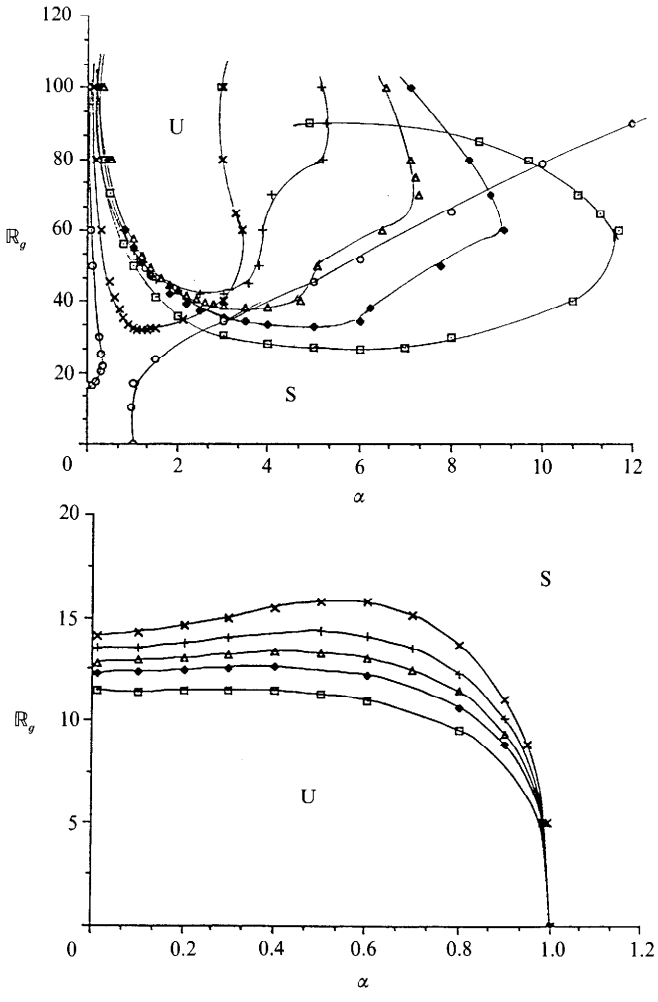

FIGURE 17. Neutral curves for $a = 1.2$, $m = 0.5$, $F = 0$, $J^* = 2000$, $\zeta_2 = 2.0$, 1.6, 1.4, 1.2, 1.0, 0.5. Symbols as for figure 16.

(2) $\mathbb{R}_L(\zeta_2)$ is a monotonically decreasing function of ζ_2 in the range of ζ_2 considered. The heavier the lubricant, the smaller is the maximum Reynolds number below which CAF is unstable to capillary instability induced by interfacial tension.

(3) $\mathbb{R}_U(\zeta_2)$ is not monotonic in ζ_2:

$$\mathbb{R}_U(1.2) > \mathbb{R}_U(1.4) > \mathbb{R}_U(1.0) > \mathbb{R}_U(1.6) > \mathbb{R}_U(2.0) > \mathbb{R}_U(0.5).$$

There is an optimal value of ζ_2, around 1.2, that maximizes $\mathbb{R}_U(\zeta_2)$.

(4) The change of $\mathbb{R}_L(\zeta_2)$ with respect to the density ratio ζ_2 is relatively small compared to that of $\mathbb{R}_U(\zeta_2)$.

(5) The stable interval (8.1) is larger when heavy fluid is outside, $\zeta_2 > 1$, than when the lighter fluid is outside, $\zeta_2 < 1$, and reaches a maximum when $\zeta_2 = 1.2$.

(6) Increasing the density of the lubricating fluid moves the upper branch towards shorter waves.

Similar conclusions can be drawn from figures 17, 18, 19 for $a = 1.2$ and 1.3, but there are some new features:

(7) When $a = 1.2$, linearly stable CAF is no longer possible for $\zeta_2 = 0.5$, while there

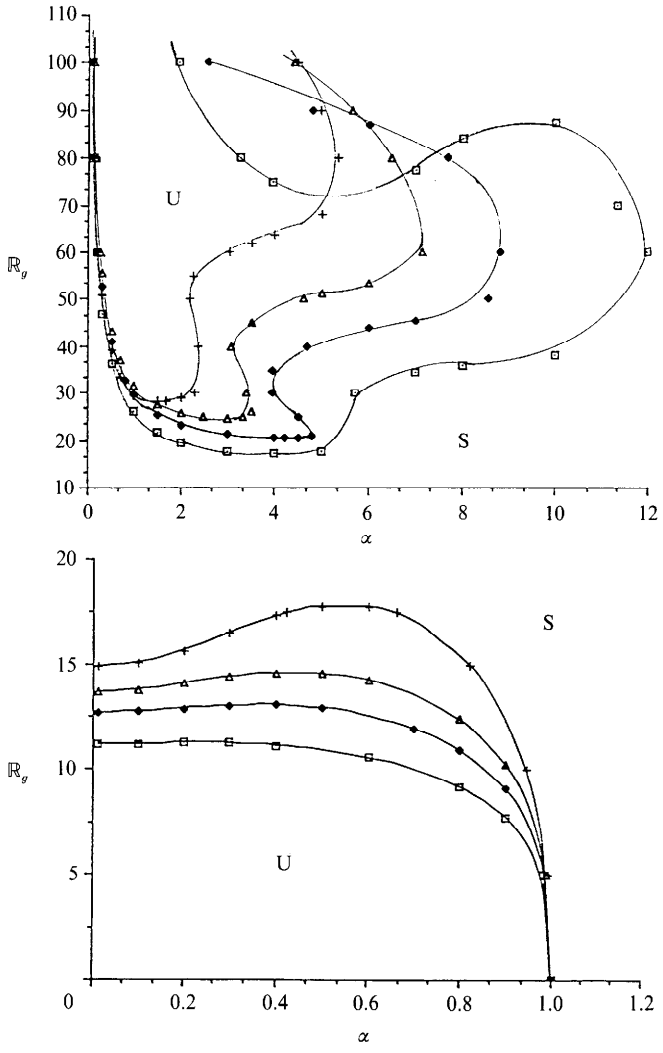

FIGURE 18. Neutral curves for $a = 1.3$, $m = 0.5$, $F = 0$, $J^* = 2000$, $\zeta_2 = 2.0$, 1.6, 1.4, 1.2. Symbols as for figure 16.

still exists a stable window of $\mathbb{R}_g$ in which CAF is stable for other density ratios $\zeta_2 = 1.0$, 1.2, 1.4, 1.6 and 2.0. When $a = 1.3$, not only $\zeta_2 = 0.5$ but also $\zeta_2 = 1.0$ become unstable, while others are still stable.

(8) The optimal value of ζ_2 which maximizes $\mathbb{R}_U(\zeta_2)$ is still about $\zeta_2 = 1.2$ for both $a = 1.2$ and 1.3.

(9) Comparing figures 16, 17 and 18, we found that, for those ζ_2 values with which there is a stable $\mathbb{R}_g$ window, and therefore $\mathbb{R}_L(\zeta_2)$ and $\mathbb{R}_U(\zeta_2)$ could be defined, the following relations hold:

$$\mathbb{R}_L(\zeta_2)|_{a=1.1} < \mathbb{R}_L(\zeta_2)|_{a=1.2} < \mathbb{R}_L(\zeta_2)|_{a=1.3}, \tag{8.2}$$

$$\mathbb{R}_U(\zeta_2)|_{a=1.1} > \mathbb{R}_U(\zeta_2)|_{a=1.2} > \mathbb{R}_U(\zeta_2)|_{a=1.3}. \tag{8.3}$$

In other words, for a fixed value of ζ_2, the size of the $\mathbb{R}_g$ window, in which CAF is stable, is a decreasing function of a.

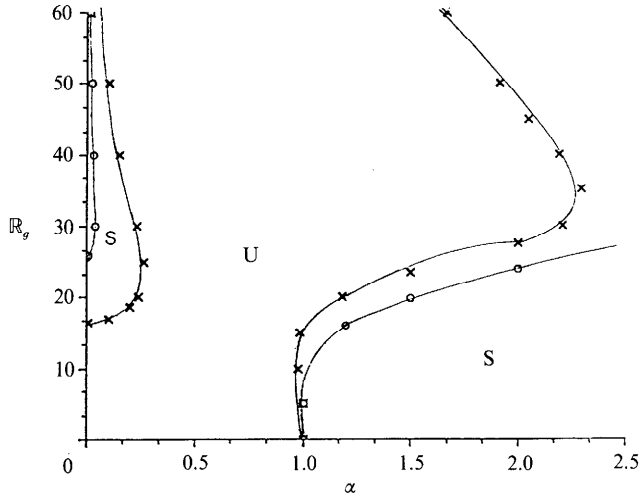

FIGURE 19. Left and right branches of neutral curves for $a = 1.3$, $m = 0.5$, $F = 0$, $J^* = 2000$, $\zeta_2 = 1.0, 0.5$. CAF is always unstable for these density ratios. Symbols as for figure 16.

The main results obtained in the study of the neutral curves for $m = 0.5$, $J^* = 2000$ can be summarized as (*a*) for a fixed value of a, there exists an optimal value of density ratio ζ_m which maximizes the size of stability window of $\mathbb{R}_g$. For the cases we computed, ζ_m is about 1.2 for $a = 1.1$, 1.2 and 1.3; (*b*) for a fixed value of ζ_2, increasing a (increasing the volume of lubricant) will decrease the size of stable window of $\mathbb{R}_g$, or even destroy the stability of the flow, like the cases $a = 1.2$, $\zeta_2 = 0.5$ and $a = 1.3$, $\zeta_2 = 0.5$, 1.0.

PCJ have shown that, other parameters fixed, there is an optimal value of viscosity ratio m which maximizes the size of the interval of Reynolds number for which CAF is stable. Using this result and those obtained above as a guideline, we designed and successfully realized perfect and stable core–annular flows in the free-fall experiment described in §3.1. The neutral curves corresponding to the example of figure 3 is given in figure 20, where the parameters $m = 0.33$, $\zeta_2 = 1.4$, $a = 1.86$, $J^* = 2.66$, and the Reynolds number for the experiment $\mathbb{R}_g = 1.82$ is shown as a dashed line. Clearly the Reynolds number for the experiment falls in the stability window of $\mathbb{R}_g$ and the experiment agrees with the linear theory.

9. Neutral curves: forced flows

In this section we shall calculate neutral curves for forced flows. We are going to explore the effects of varying the density ratio on lubricating layers $a = 1.1$, 1.2, 1.3 and 1.4 for a sample set of parameters $m = 0.5$, $J^* = 2000$, $\mathbb{R}_g = 10$.

Neutral curves for $a = 1.1$ are shown in figure 21. For each value of ζ_2, there are three branches of neutral curves. A region of capillary instability to long waves is formed for slow motions around $F = -1$. This region is shown in (*b*). When $\zeta_2 = 1$, all the neutral curves are symmetric about the axis $F = -1$. Since the basic flow is symmetric about $F = -1$, changing the value of F from F_1 to $-F_1 - 2$ will only reverse the flow without changing the dynamics. Figure 21(*b*) shows that heavier lubricants will shift the region of capillary instability downward without changing its shape. Therefore, for a given pressure gradient, one way to overcome the capillary instability is to use heavy lubricant for down-flows (say $F > 0$) or light lubricant for

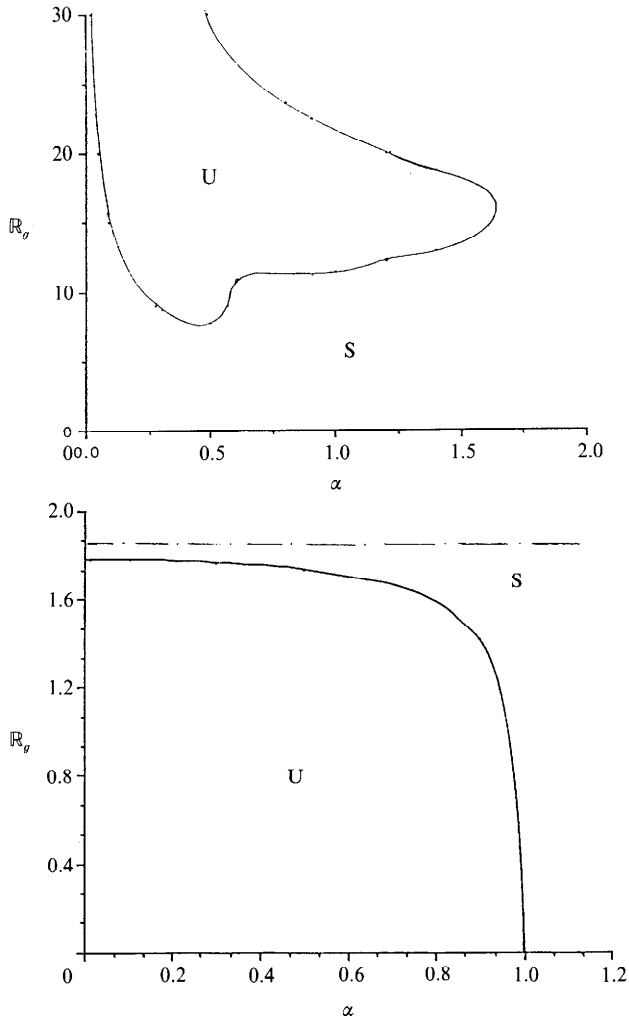

FIGURE 20. Neutral curves for free fall, $a = 1.86$, $m = 0.33$, $\zeta_2 = 1.4$, $J^* = 2.26$, $F = 0$. Stable and unstable regions are marked by S and U respectively. The dashed straight line corresponds to the experiment $\mathbb{R}_g = 1.82$, which is shown in figure 3. Stable perfect core–annular flow is observed.

up-flows (say $F < -1$). This result counters the heuristic idea that the heavier fluid should tend to stay at the centre of the pipe for down-flows and with light fluid at the centre for up-flows. Renardy (1987) has already demonstrated for some cases that this common intuition is wrong for plane vertical Poiseuille flow of two fluids.

The upper branches (a) of the neutral curves correspond to fast flow. The effect of increasing ζ_2 on the top curve of figure 21(a) is interesting. We may confine our remarks to the positive upper branch (F being positive) since the negative upper branch (F being negative) is dynamically similar to the positive one with the sign of F reversed. Similar to the case of free fall under gravity, for a given value of a, there is an optimizing value ζ_m of the density ratio ζ_2, for with $F_U(\zeta_m)$ is a maximum, where $F_U(\zeta_2)$ is the minimum value of $F(\alpha)$ on the upper neutral curve over α for each fixed value ζ_2. For $a = 1.1$, ζ_m is about 1.5. The upper branch (a) is more sensitive than the capillary branch (b) to changes of ζ_2. When ζ_2 is increased the unstable wavenumbers on the upper branches (a) are shifted to shorter waves, larger α.

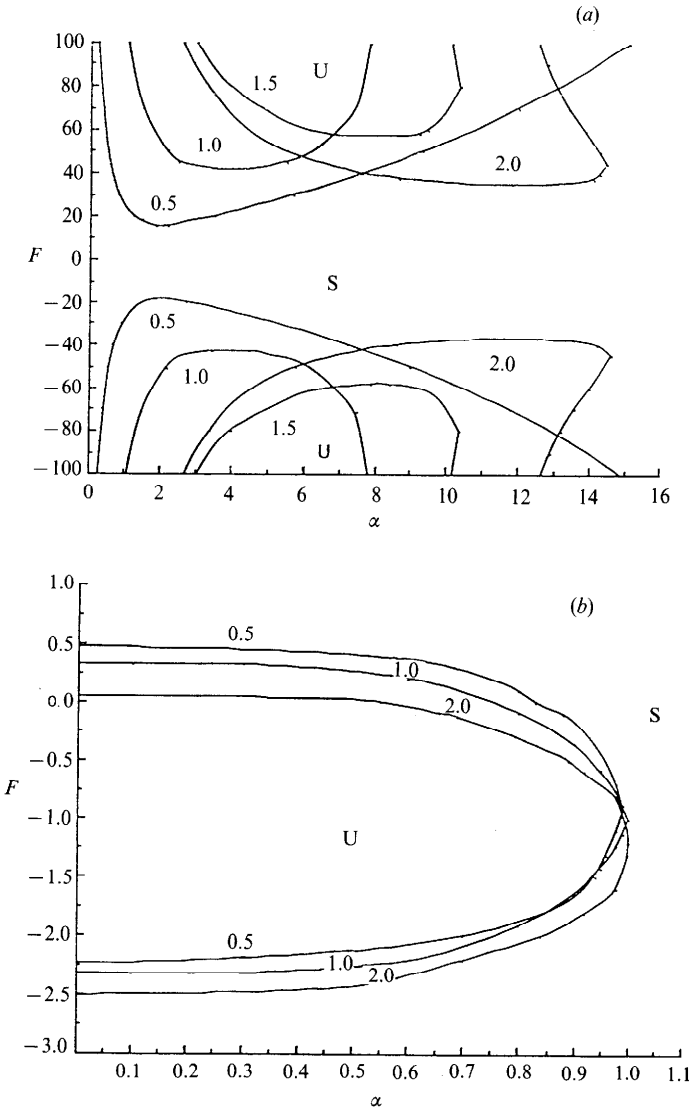

FIGURE 21. Neutral curves for $a = 1.1$, $m = 0.5$, $J^* = 2000$, $\mathbb{R}_g = 10$, and different values of ζ_2 given by the numbers above each curve. (*a*) Upper positive and negative F branches. The negative branches are similar to the positive ones. The band of stable region is maximized for a certain value ζ_m of ζ_2, and ζ_m is close to 1.5. (*b*) Regions of capillary instability.

Figure 22 gives the neutral curves for $a = 1.2$. For each given value of ζ_2, the size of stable regions for CAF are rapidly reduced as the water fraction is increased. For $\zeta_2 = 0.5$, stable CAF is impossible for $a = 1.2$, while for $a = 1.1$ there is still a region of stability. The main effect of increasing a is to move the upper branches downward, reducing the region of stability. The lower branch of the neutral curve is less sensitive to changing a. The upper branch sinks as a is increased until it connects with the lower branch at a critical value of a. Then stable CAF is not possible. The critical value of a depends strongly on all the other parameters.

The neutral curves for negative values of F in figure 22(*a*) are nearly mirror reflections of the upper branches of neutral curves for positive F across the line

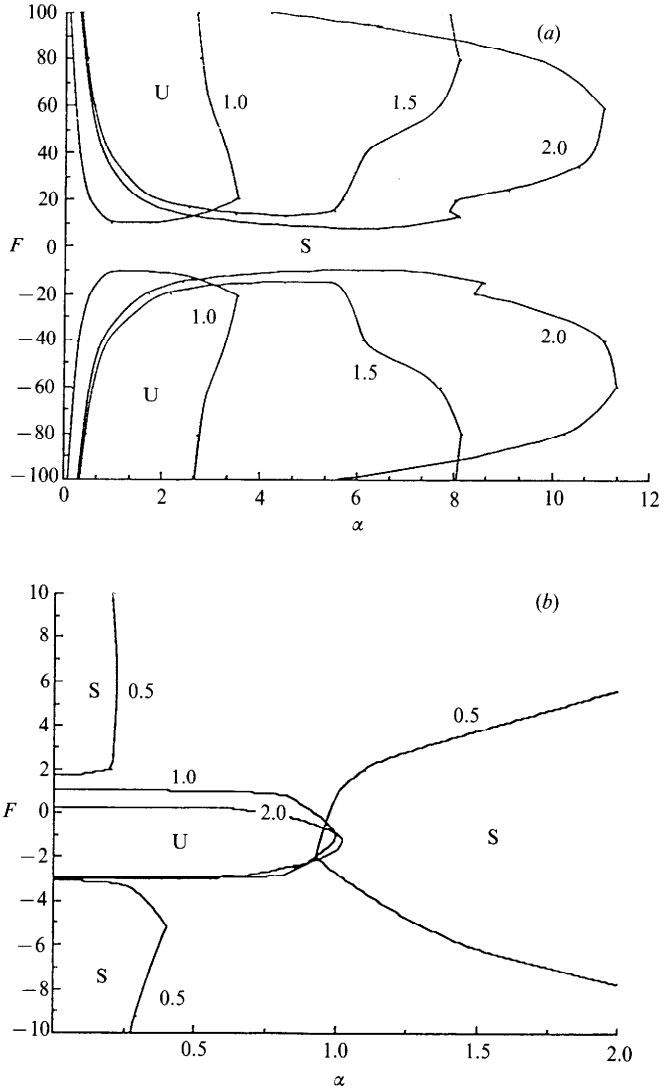

FIGURE 22. Neutral curves for $a = 1.2$, $m = 0.5$, $J^* = 2000$, $\mathbb{R}_g = 10$, and different values of ζ_2. (*a*) Positive and negative F upper branches. The stability regions are largest when the density ratio ζ_2 is close to 1.5. (*b*) Detailed view near the capillary instability region. The neutral curves for $\zeta_2 = 0.5$ are also shown here. CAF is always unstable for $\zeta_2 = 0.5$.

$F = -1$. We call these 'negative-F upper branches'. The negative-F upper branches shift to short waves as ζ_2 is increased more strongly than the positive branches (see figure 22*a*). There is again a density ratio which maximizes stability.

Figure 23 shows that when the density is matched stable CAF is possible when the radius ratio $a \leqslant 1.2$, but is not possible for $a = 1.3$. Stable CAF can be achieved when a is large by choosing a lubricant which brings the density ratio close to the optimal one, stability for $a = 1.3$ when $\zeta_2 = 2$ and instability when $\zeta_2 = 0.5$.

Very similar to the free-fall situation discussed in §8, for a given a, the largest window of stable CAF can be achieved by choosing a favourable density ratio ζ_m, and for a given density ratio ζ_2, the size of the stable region can be reduced by increasing the radius ratio a. For example, the stabilization of the flow for $a = 1.3$, achieved by

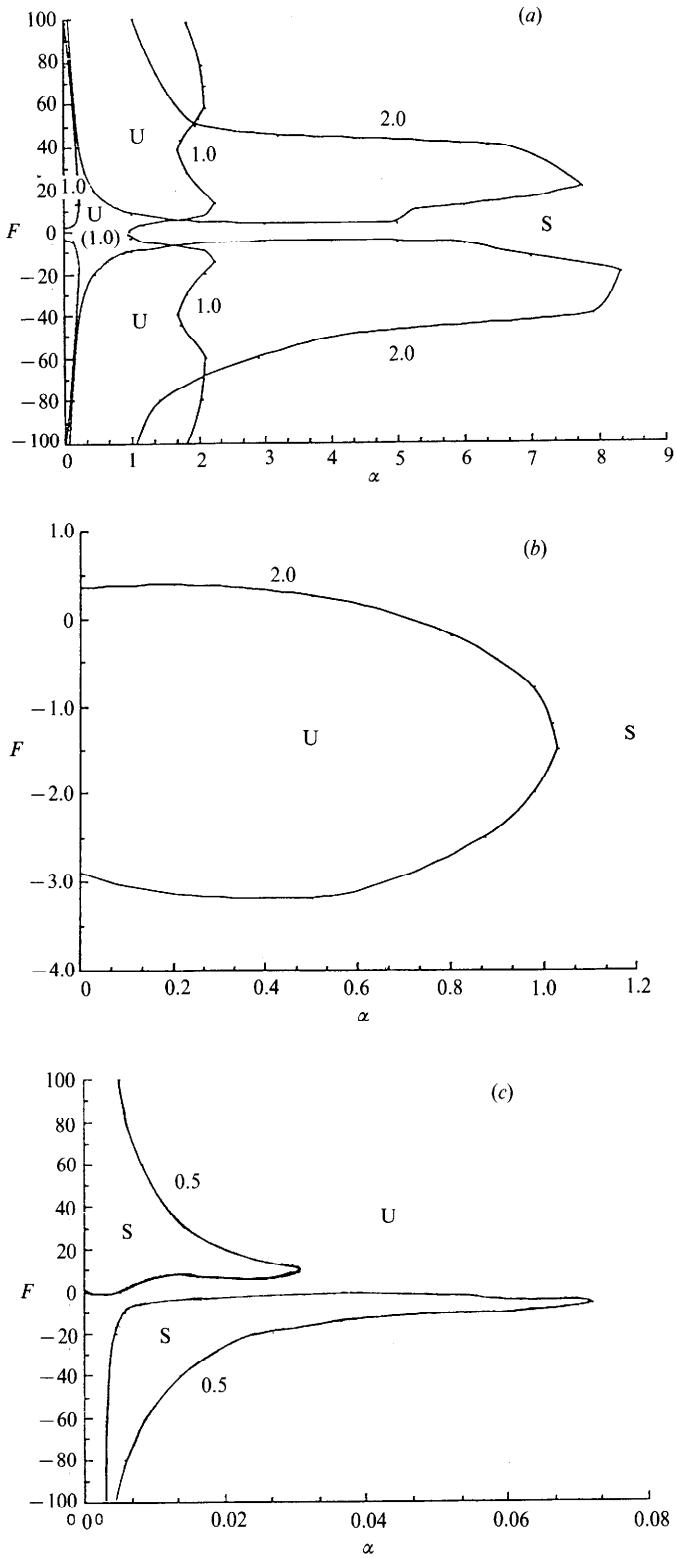

FIGURE 23(*a–c*). For caption see facing page.

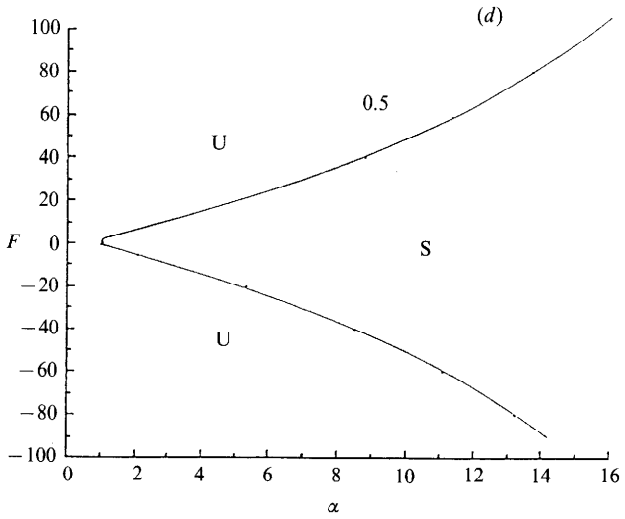

FIGURE 23. Neutral curves for $a = 1.3$, $m = 0.5$, $J^* = 2000$, $\mathbb{R}_g = 10$, and different values of ζ_2. Stable CAF is hard to achieve. (*a*) A global view. (*b*) Region of capillary instability for $\zeta_2 = 2.0$. (*c*) Left branch for $\zeta_2 = 0.5$: it consists of two parts. (*d*) Right branch for $\zeta_2 = 0.5$.

increasing the density ratio to $\zeta_2 = 2$ (figure 23*a*), is nearly lost when a is increased to 1.4 (figure 24*d*). The figures show that the destabilization with increasing lubricant fraction (or radius ratio a) acts on the upper branch of the neutral curve and can be countered by a suitable choice of $\zeta_2 = \zeta_m$, where ζ_m is the most favourable density ratio. We may have stability, even with large a, by a strategic choice of ζ_2.

10. Conclusions

We have analysed the effects of the density difference on the stability of vertical core–annular flow. The density difference changes the basic flow and introduces an effective gravity $[\![\rho]\!]g$ in the balance equation for the shear stress at the interface.

First we summarize the main results for free fall when the lubricating layer is thin and the viscosities are matched, $(F, a, m) = (0, 1.1, 1)$, emphasizing the effect of the density ratio.

(1) Energy analysis shows that interfacial gravity is destabilizing, for heavy and light lubricants and at all Reynolds numbers.

(2) The Reynolds stress minus the dissipation is stabilizing in all the cases we computed.

(3) The stabilizing effects just mentioned are in opposition to capillary instability and to the destabilizing effects of gravity at the interface which drive the fluids to vertical stratification. The flow may be stabilized by dissipation for $\mathbb{R} > \mathbb{R}_c(\zeta_2)$ if the lubricant is heavy, but not if it is light.

Now we allow for different viscosities with the more viscous fluid inside, as usual, $m = 0.5$.

(4) Heavy lubricants suppress capillary instability. Increasing the density of the lubricant shifts the upper branch of the neutral curves towards shorter waves.

(5) When the lubricating layer is thin and the density ratio is not too small, there is an interval of Reynolds numbers between the lower and upper branches in which CAF is stable.

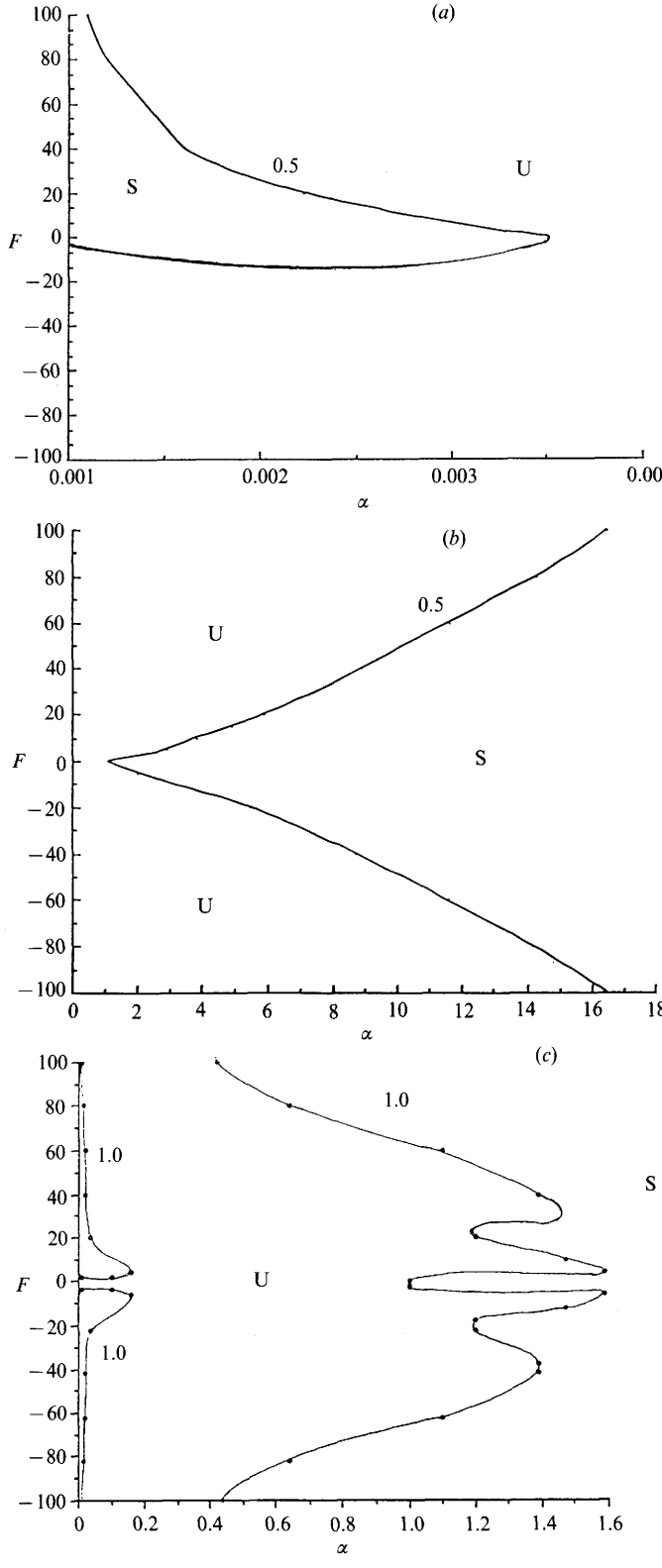

FIGURE 24(*a–c*). For caption see facing page.

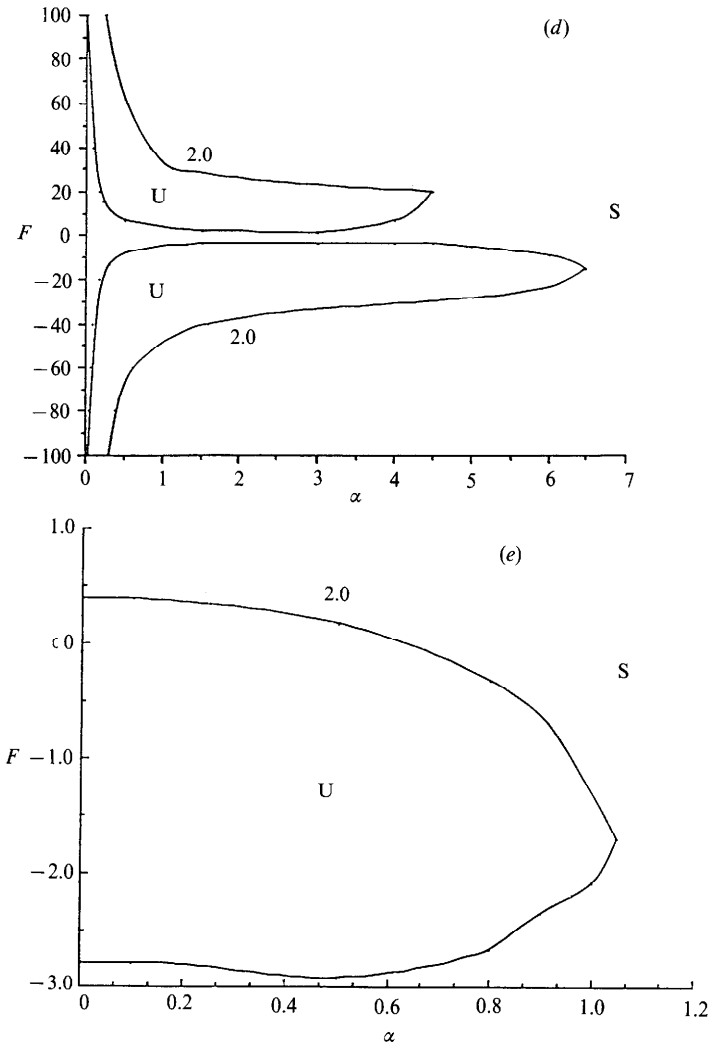

FIGURE 24. Neutral curves for $a = 1.4$, $m = 0.5$, $J^* = 2000$, $\mathbb{R}_g = 10$ and various ζ_2. (*a*) Left branch for $\zeta_2 = 0.5$. (*b*) Right branch for $\zeta_2 = 0.5$. CAF is always unstable. (*c*) $\zeta_2 = 1$. CAF is always unstable. (*d*) Positive and negative upper branches for $\zeta_2 = 2$. There is a narrow band of stability. (*e*) Region of capillary instability for $\zeta_2 = 2$.

(6) For a given value of a, we can maximize the interval of Reynolds numbers on which CAF is stable by choosing a best $\zeta_2 = \zeta_m$, $0 < \zeta_m < \infty$, the other parameters being fixed. The destabilization of the upper branch due to increasing a, thick lubricating layers, can be countered by using lubricants with ζ_2 close to ζ_m.

In the case of forced flow, $F \neq 0$ and F can be positive or negative. When $\zeta_2 = 1$, $F = -1$ implies that the gravity force and the pressure gradient are in balance and the neutrally buoyant core flow will break up by capillary instability. Large positive F means down-flow, negative F means up-flow. There are two branches of neutral curves for up-flow and two branches for down-flow, the capillary branch and the upper branch.

(7) To achieve stable CAF for slow flow, use a heavy lubricant for down-flow and a light one for up-flow.

(8) The difference between up-flow and down-flow decreases with $|F|$.

(9) The upper branch for up-flow and down-flow is more sensitive to changes in the density of the lubricant than the capillary branch. Increasing the density of the lubricant will shift all the upper branches to shorter waves.

(10) Other parameters being fixed, there is an optimizing density ratio $\zeta_2 = \zeta_m$ which gives the largest interval of Reynolds numbers for stability. It follows, for example, that the thickest stable lubricating layer is the one for which $\zeta_2 = \zeta_m$.

Our experiments on free fall have established that it is possible to run a perfect core–annular flow, robustly stable to finite-amplitude disturbances if the operating conditions are stable according to linearized theory. There is a huge amount of information which can be obtained from experiments on forced flow. Some preliminary results given here are enough to show range of flows which can be expected from a heavy motor oil and water. The hold-up ratio proves to be an important parameter in determining the operating water fraction. Water accumulates in up-flow because effective gravity accelerates oil and decelerates water. For down-flow, the opposite is true, gravity accelerates water and decelerates oil. We therefore get a greater accumulation of water in up-flow. This fact appears to explain the differences observed in up- and down-flow in figure 6.

We intend to prepare flow charts for forced flow with superficial velocities, pressure gradients and hold-up ratios for different oils and to compare the observations with linear theory in a future publication.

This work is supported by the Army Research Office, Mathematics; the Department of Energy; the National Science Foundation, Fluid Mechanics and the Minnesota Supercomputer Institute. R. Bai's work is supported by the People's Republic of China. We are indebted to Howard Hu for his help with our energy calculation.

Appendix

In the long-wave limit $\alpha \to 0$, the eigenvalue problem can be solved explicitly in power series of α. The eigenvalue

$$c = c^{(0)} + \alpha c^{(1)} + O(\alpha^2).$$

It is found that $c^{(0)}$ is real and thus does not affect the stability:

$$W(1) - c^{(0)} = \frac{(a^2-1)^2}{2(a^4+m-1)}[\![W'(1)]\!] + \frac{2(a^4+m-1)\ln a - (a^2-1)(m+2a^2-2)}{4m(a^4+m-1)}[\![m_i W''(1)]\!],$$

where $m_1 = 1$ and $m_2 = m$. At the next order, $O(\alpha)$, $c^{(1)}$ is found to be purely imaginary and can be expressed as

$$c^{(1)} = \mathrm{i}\left\{\frac{J^*}{\mathbb{R}} f_1(a, m) + \mathbb{R} f_2(a, m, \zeta_2, F)\right\}.$$

The function $f_1(a, m)$ is definite positive and can be written as

$$f_1(a, m) = G_2/G_1 > 0,$$

where

$$G_1 = 8192 a^2 m^2 (a^4 + m - 1)^2 > 0,$$

$$G_2 = 512 am\{m(a^4 - 4a^2 + 3 + 4\ln a) + 4(a^2-1)[(a^2+1)\ln a + 1 - a^2]\} > 0.$$

To define the function $f_2(a, m, \zeta_2, F)$, we have to first define the following parameters:

$$W(1) = \frac{F+\zeta_2}{4m}(a^2-1)+\frac{1-\zeta_2}{2m}\ln a, \quad [\![W'(1)]\!] = \frac{1-m}{2m}(F+1), \quad [\![m_1 W''(1)]\!] = \zeta_2-1,$$

$$[\![\zeta_1 W'(1)]\!] = \frac{(\zeta_2-m)F+2\zeta_2^2-\zeta_2-m}{2m}, \quad \beta_{11} = \tfrac{1}{4}(F+1), \quad \beta_{12} = \beta_{11}+W(1),$$

$$\beta_{21} = \frac{F+\zeta_2}{4m}, \quad \beta_{22} = \frac{1-\zeta_2}{2m}, \quad \beta_{23} = \beta_{21}a^2+\beta_{22}\ln a,$$

$$A_1 = 64am^2[\![W'(1)]\!]+32am(a^2-1)[\![m_1 W''(1)]\!],$$

$$A_3 = 64am\{(a^2-1)^2-m\}[\![W'(1)]\!]-64a\{(a^2-1)(a^2+m-1) - (a^4+m=1)\ln a\}[\![m_1 W''(1)]\!],$$

$$B_1 = 64am[\![W'(1)]\!]+32a(a^2-1)[\![m_1 W''(1)]\!], \quad B_2 = -64a(a^4+m-1)[\![m_1 W''(1)]\!],$$

$$B_3 = -128a^3m[\![W'(1)]\!]-32a\{(a^2-1)^2-m-2(a^4+m-1)\ln a\}[\![m_1 W''(1)]\!],$$

$$B_4 = 64a^5m[\![W'(1)]\!]-32a^3(a^2+m-1)[\![m_1 W''(1)]\!],$$

$$E_{11} = 4am(a^2-1)^2, \quad E_{12} = -8a\{(a^2-1)[(a^2-2)m-2(a^2-1)]+2(a^4+m-1)\ln a\},$$

$$E_{21} = -4a[m+2(a^2-1)], \quad E_{22} = 16a(a^4+m-1),$$

$$E_{23} = -8a\{2(a^4+m-1)\ln a-(a^2-1)(a^2+m-1)\}, \quad E_{24} = -4a^3\{a^2m-2(a^2+m-1)\}.$$

Then we define:

$$G_3 = (E_{11}+E_{12})\{(W(1)-c^{(0)})[4A_1+2A_3-\zeta_2(4B_1+B_2+2B_3)]-[\![\zeta_1 W'(1)]\!](A_1+A_3)\},$$

$$II_1 = A_1\{E_{11}(-\beta_{11}+\tfrac{4}{3}\beta_{12}-\tfrac{4}{3}c^{(0)})+E_{12}(-\tfrac{4}{3}\beta_{11}+2\beta_{12}-2c^{(0)})\},$$

$$II_2 = \sum_{j=1}^{4}\sum_{i=1}^{4} B_j E_{2i} h_{ji},$$

where h_{ji} are given by

$$h_{11} = \tfrac{1}{3}(4\beta_{23}-4c^{(0)}-\beta_{22})(a^6-1)-\beta_{21}(a^8-1)-\tfrac{1}{4}\beta_{22}(6a^6\ln a-a^6+1),$$

$$h_{12} = \tfrac{1}{8}(4\beta_{23}-4c^{(0)}-\beta_{22})(4a^4\ln a-a^4+1)-\tfrac{1}{4}\beta_{21}(6a^6\ln a-a^6+1) - 2\beta_{22}\{a^4(\ln a)^2-\tfrac{1}{8}(4a^4\ln a-a^4+1)\},$$

$$h_{13} = \tfrac{1}{2}(4\beta_{23}-4c^{(0)}-\beta_{22})(a^4-1)-\tfrac{4}{3}\beta_{21}(a^6-1)-\tfrac{1}{2}\beta_{22}(4a^4\ln a-a^4+1),$$

$$h_{14} = (4\beta_{23}-4c^{(0)}-\beta_{22})(a^2-1)-2\beta_{21}(a^4-1)-2\beta_{22}(2a^2\ln a-a^2+1),$$

$$h_{21} = \tfrac{1}{2}(\beta_{23}-c^{(0)})(a^4-1)-\tfrac{1}{3}\beta_{21}(a^6-1)-\tfrac{1}{4}\beta_{22}(4a^4\ln a-a^4+1),$$

$$h_{22} = \tfrac{1}{2}(\beta_{23}-c^{(0)})(2a^2\ln a-a^2+1)-\tfrac{1}{8}\beta_{21}(4a^4\ln a-a^4+1) - \beta_{22}[2a^2(\ln a)^2-2a^2\ln a+a^2-1)],$$

$$h_{23} = (\beta_{23}-c^{(0)})(a^2-1)-\tfrac{1}{2}\beta_{21}(a^4-1)-\beta_{22}(2a^2\ln a-a^2+1),$$

$$h_{24} = 2(\beta_{23}-c^{(0)})\ln a-2\beta_{21}(a^2-1)-2\beta_{22}(\ln a)^2,$$

$$h_{31} = -\tfrac{1}{2}\beta_{22}(a^4-1), \quad h_{32} = -\tfrac{1}{2}\beta_{22}(2a^2\ln a-a^2+1), \quad h_{33} = -\beta_{22}(a^2-1),$$

$$h_{34} = -2\beta_{22}\ln a, \quad h_{41} = -2\beta_{22}\ln a,$$

$$h_{42} = -\beta_{22}(\ln a)^2, \quad h_{43} = -2\beta_{22}\ln a, \quad h_{44} = -\beta_{22}\frac{a^2-1}{a^2}.$$

Now the function $f_2(a, m, \zeta_2, F)$ is given by

$$f_2(a, m, \zeta_2, F) = \frac{II_1 + II_2 - G_3}{G_1}.$$

And it is easy to see that other parameters fixed, $f_2(a, m, \zeta_2, F)$ is quadratic polynomial of ζ_2.

REFERENCES

CHANDRASEKHAR, S. 1961 *Hydrodynamics and Hydromagnetic Stability*. Dover.

CHARLES, M. E., GOVIER, G. W. & HODGSON, G. W. 1961 The horizontal pipeline flow of equal density oil-water mixtures. *Can. J. Chem. Engng* **39**, 17–36.

HICKOX, C. E. 1971 Instability due to viscosity and density stratification in axisymmetric pipe flow. *Phys. Fluids* **14**, 251–262.

HU, H. & JOSEPH, D. D. 1989 Lubricated pipelining: stability of core–annular flow. Part 2. *J. Fluid Mech.* **205**, 359–396 (referred to as HJ).

JOSEPH, D. D., RENARDY, M. & RENARDY, Y. 1984 Instability of the flow of immiscible liquids with different viscosities in a pipe. *J. Fluid Mech.* **141**, 319–345 (referred to as JRR).

LISTER, J. R. 1987 Long-wavelength instability of a line plume. *J. Fluid Mech.* **175**, 413–428.

PREZIOSI, L., CHEN, K. & JOSEPH, D. D. 1989 Lubricated pipelining: stability of core–annular flow. *J. Fluid Mech.* **201**, 323–356 (referred to as PCJ).

RENARDY, Y. 1987 Viscosity and density stratification in vertical Poiseuille flow. *Phys. Fluids* **30**, 1638–1648.

YIH, C. S. 1967 Instability due to viscosity stratification. *J. Fluid Mech.* **27**, 337–352.